Force-Directed Control with a Strong Hydraulic Manipulator

by

Peter Carl Lefren Jaffe

Submitted to the Department of Electrical Engineering and Computer Science

in Partial Fulfillment of the Requirements for the Degree of

Master of Engineering in Electrical Engineering and Computer Science

at the Massachusetts Institute of Technology

February 3, 1999

Signature of Author _____

Department of Electrical Engineering and Computer Science
January 22, 1999

Certified By _____

Steven Dubowsky
Thesis Supervisor

Accepted By _____

Arthur C. Smith
Chairman, Departmental Graduate Committee

Force-Directed Control with a Strong Hydraulic Manipulator
by
Peter Carl Lefren Jaffe

Submitted to the
Department of Electrical Engineering and Computer Science

February 3, 1999

In Partial Fulfillment of the Requirements for the Degree of
Master of Engineering in Electrical Engineering and Computer Science

ABSTRACT

The nuclear maintenance task of nozzle dam placement lends itself to investigations in robotic automation. This task involves insertion of a heavy payload within tight tolerances and requires the use of a strong, inherently imprecise manipulator, such as the Schilling Titan II hydraulic robot.

To address the challenge of automating this task, an experimental system is designed to allow development of advanced control methods and an operator interface.

A Base Sensor Control (BSC) algorithm is applied in concert with a Geometric and Elastic Error Correction (GEC) method to improve manipulator absolute accuracy. Experimental data supports that the repeatability and absolute position accuracy achieved the resolution of the position sensors.

A virtual environment teleoperation application is presented. It was implemented by integrating a 3-D kinematic simulation of the manipulator with the control computer. This interface provides improved visualization of the workspace.

The use of force information to aid in insertion is explored. For known geometries, a method is developed for estimating contact points using a wrist force/torque sensor. The use of this information in the teleoperation application and automatic placement algorithms is explored.

Thesis Supervisor: Dr. Steven Dubowsky
Title: Professor of Mechanical Engineering

Acknowledgements

I would like to thank Professor Steven Dubowsky for his insight, ideas, and guidance during my time with the Field and Space Robotics Laboratory. I would also like to thank the other members of the FSRL who made my experience an educational and enjoyable one.

In particular, I would like to thank my colleagues Karl Iagnemma and Marco Meggiolaro as well as Dr. Byung-Hak Cho of the Korean Electric Power Research Institute (KEPRI) for their invaluable help in our joint effort to achieve success with the nozzle dam project. Also, Chad Souke and Socrates Gomez contributed great insight and considerable time in building components of the experimental testbed.

This thesis describes research performed at the MIT Field and Space Robotics Laboratory under the sponsorship of the Korean Electricity and Power Company and Electricité de France. Thanks to KEPCO and EDF for providing the financial support for this project.

My parents, Carl and Toini, and brother, Jud, have been loving and supportive throughout the course of my research and life. If ever things don't go the way I think they should, they are always there to lend me confidence and laughs.

Each evening with my soon-to-be wife, Adrienne, allowed me to return to MIT the following day happy with my life. I definitely could not have done it without you. And, since you already wrote your MEng. thesis, you just told me all the answers.

Table of Contents

List of Figures

List of Tables

Chapter 1

Introduction

1.1 Background

There are many industrial tasks for which human operators are not well suited. This may be due to the tedious or repetitive nature of the tasks, or else harsh or dangerous conditions might place undue stress on the personnel. The nuclear industry has many such tasks, often due to the prevalence of radiation in the work site. Robotics provide alternate methods for completing these tasks while eliminating many of the work related hazards.

One specific case of harsh conditions is in pressurized water reactor nuclear power plants where workers, who are referred to as "jumpers," perform the dangerous task of steam generator maintenance. Once a year, each nuclear reactor is shutdown for a month to swap old fuel rods in the reactor core with new ones (Figure 1 shows a graphical overview of the process for a Westinghouse type F steam generator). At the same time the fuel is replenished, the U-tubes in the steam generator must be inspected for damage. In order for workers to enter the steam generator, the water in the reactor core must be prevented from entering the steam generator's water chamber. This is achieved by covering the two large portals (one meter in diameter) that connect the hot and cold pipes to the steam generator (Cho, 1997). Each portal has a nozzle ring into which a device referred to as a nozzle dam is inserted with a tolerance of approximately 1 mm. The nozzle dam is installed in two phases. The first involves fitting the nozzle dam side plate in the nozzle ring (Figure 2a), and then the nozzle dam center plate is placed

within the side plate (Figure 2b). This provides the necessary seal to prevent water leakage, thereby allowing workers to enter the steam generator and inspect the U-tubes.

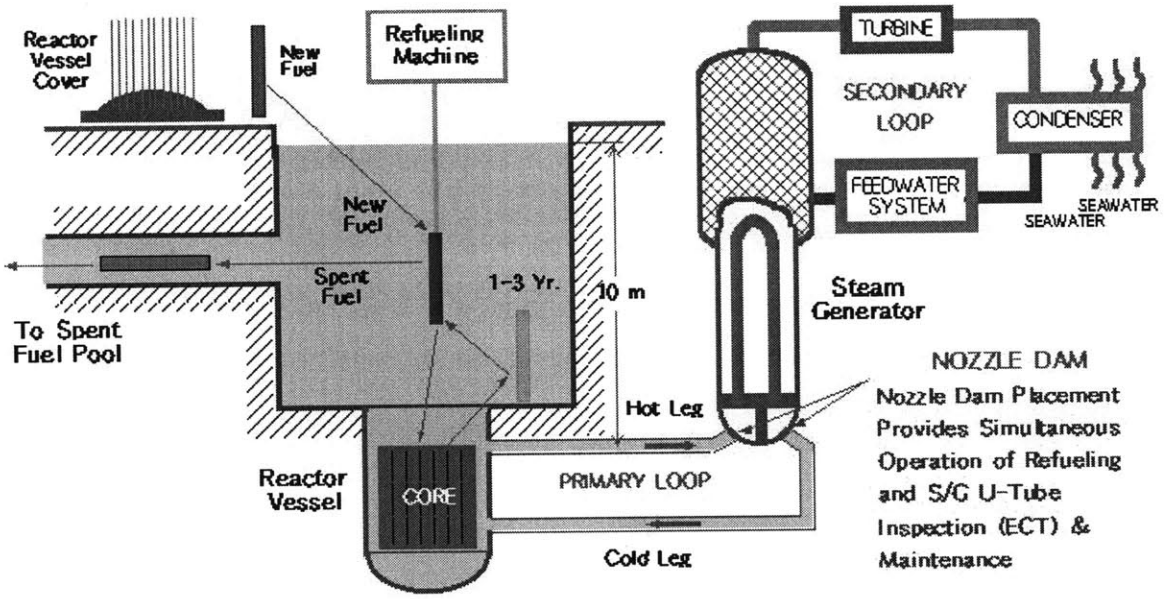

Figure 1 - Nuclear Reactor (Cho, 1998)

Installing one nozzle dam requires hours of manual labor during which time the workers are exposed to high doses of residual radiation. Jumpers can only remain in the steam generator chamber for three minutes before receiving their maximum acceptable radiation dosage for the year. At this point, the worker leaves the chamber through the 0.4 m (15.7") in diameter access portal and another worker enters to resume the task (Zezza, 1985). The manpower and time required to complete this task, as well as the health risks imposed on the workers, makes this task well suited to investigations in automation. Recent attempts to place the nozzle dam with a manipulator have taken very long because of the combination of lack of manipulator accuracy and poor operator visibility. Successful completion of the task with a manipulator would eliminate radiation exposure as well as save money by reducing the time required to place the nozzle dam. For each hour that the reactor is off line, $40,000 in potential revenues is

lost. The key to performing this task with robotic manipulators is improving both manipulator accuracy and the operator interface.

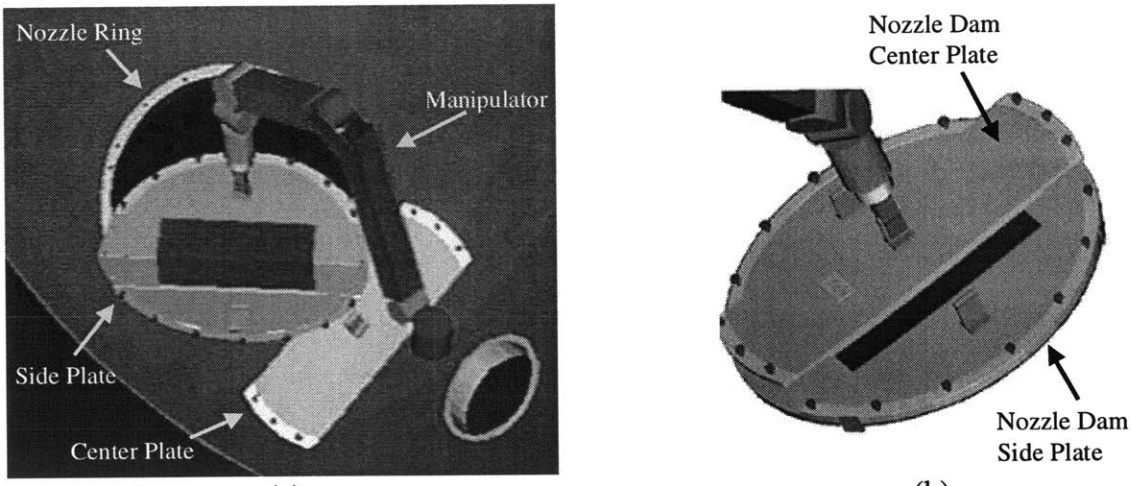

Figure 2 - Simulated Robotic Nozzle Dam Task

1.2 Literature Review

The nozzle dam placement problem can be viewed as a specific example of the classic peg-in-the-hole insertion problem. However, it involves positioning a large, heavy rectangular peg in a harsh environment using an inherently inaccurate manipulator. It is widely accepted that force information is critical in performing classic high tolerance peg-in-the-hole insertions (Gorinevsky, 1997). Methods typically use either passive or active accommodation systems.

Many methods have been established to accomplish insertion by passive accommodation. The most common of these methods uses either a compliant wrist or a random search pattern (Qiao, 1995). By providing a compliant mounting for the peg, the insertion process can be successful even when an initial position error is present. The compliance allows contact forces to realign the peg with the hole without requiring repositioning of the manipulator. However, this method requires that the initial error be

no greater than the size of any chamfer on the mating parts, otherwise, the resulting contact forces would not aid in peg and hole alignment most likely resulting in jamming.

Active force control assumes that the manipulator can position the peg within a bounded region around the hole so that measured contact forces and moments can be used to aid in the insertion process (Nevins, 1973). Active accommodation methods include augmenting position feedback based on interpreted force information, learning algorithms (Gullapalli, 1992), and nullifying strategies (Simunovic, 1979). These systems require additional hardware, such as a wrist force/torque sensor, and impose a considerable additional computation load on the control computer. However, active accommodation algorithms will tend to be more error tolerant than passive methods.

In addition, there has been considerable work in the field of virtual environments and teleoperation. Virtual environments improve teleoperation capabilities by providing ideal operator viewpoints and allowing visual display of trajectories in the virtual world (Lee, 1997). Research has also been conducted to evaluate the use of visual force feedback for teleoperated insertion tasks. One work presents a 6-D docking problem where operators are evaluated while using visual displays with and without force visualization (Ming, 1984).

However, the practical use of large strong manipulators to perform accurate placement of large heavy objects, such as in the nozzle dam problem, has yet to be demonstrated. The nozzle dam problem is very difficult due to the tight insertion tolerances, the weight of the nozzle dam, and the confined and dangerous operating environment. The high tolerances and the heavy weight require that a powerful, but accurate, manipulator be used to achieve the task. A major limiting factor of strong

manipulators is that they inherently have poor repeatability and poor absolute accuracy. The nozzle dam problem is made even more difficult by the lack of direct visibility of the insertion surfaces, hence teleoperation is not the simple solution to the problem.

1.3 Purpose of this Thesis

The purpose of this thesis is to investigate the application of a manipulator to the nozzle dam placement process. MIT's Field and Space Robotics Laboratory had recently developed control techniques that demonstrated drastically improved repeatability of robotic manipulators using a method call Base Sensor Control or BSC (Morel, 1996). Methods to correct for geometric and elastic errors in large manipulators have also recently been a result of the laboratory's research in medical robotic systems (Drouet 1998, Meggiolaro 1998). The nozzle dam task was seen as a problem that could benefit from this line of research in high accuracy positioning of strong manipulators. The objective of this research became the exploration of using a robotic manipulator to complete the hazardous nuclear maintenance task of nozzle dam placement, which is currently accomplished by human workers.

This presented the opportunity to extend high precision control algorithms to a Schilling Titan II strong hydraulic manipulator, which is an industry standard for maneuvering heavy payloads in harsh environments. The operating environment precludes the presence of humans in the workspace to provide path planning. Also, a teleoperator would have difficulty performing such high tolerance insertions using standard cameras and television monitors. Therefore, the research was extended to include virtual environments and how they can be applied to manipulator control. The design of the operator interface is crucial in providing the operator with both powerful

and useful control of the manipulator. This involves considering how the task status is presented to the user as well as how one would pass commands to the control algorithm.

In this research, it was also found that increased manipulator absolute accuracy and a comprehensive operator interface may not be sufficient for completing the task. Many sources of error can contribute to uncertainties in the mating geometry from which pure position control algorithms can not recover. To resolve this problem, a method of calculating contact forces was used to provide critical data to allow successful completion of the nozzle dam insertion task. Use of the contact information was explored for both teleoperator and automated placement approaches.

1.4 Outline of this Thesis

This thesis is divided into six chapters. This chapter serves as an introduction and overview of the work. Chapter 2 introduces both the mechanical and electrical aspects of the experimental system. The Schilling manipulator used in this research is described. Then, the experimental fixture used to research the nozzle dam task is presented. After discussing the original control electronics, the modified electrical system is outlined.

Chapter 3 presents the methods by which high position accuracy is achieved on the Schilling manipulator. The theory of Base Sensor Control (BSC) is reviewed and experimental data is given supporting significant repeatability improvements. Geometric and Elastic Error Compensation (GEC) is then discussed, and its application to the Schilling is evaluated. Finally, the two algorithms are applied in concert, and experimental results are presented demonstrating that absolute accuracy has been improved to the order of the system's position sensing resolution.

Chapter 4 introduces a virtual environment teleoperator interface. The system grew out of a 3-D kinematic simulation program written to analyze the nozzle dam task. This system was then integrated with control hardware to provide a comprehensive teleoperation package.

Chapter 5 discusses the application of force information to the control system. First a method for resolving contact information is presented. The contact information is integrated into the teleoperation interface to aid the operator in completing the insertion task. Also, the use of contact information in automated insertion simulations is discussed.

Chapter 6 summarizes the conclusions regarding the development of a force-directed controller for achieving nozzle dam placement with a strong hydraulic manipulator. Finally, suggestions for further work are presented.

The appendices to this thesis give detailed information on specific topics related to the practical implementation of the work presented. Appendix A provides code specifications for the PC VME link interface. Appendix B contains pin-out information for the wiring of the wrist force/torque sensor.

Chapter 2

Experimental Hardware

An appropriate experimental system was developed to investigate automation of the nozzle dam insertion task. Certain existing hardware in the Field and Space Robotics Laboratory lent itself to the task, however substantial additional components were added to construct a nozzle dam experimental testbed. The final system is a blend of mechanical and electrical components.

2.1 Mechanical System

The mechanical system can be broken down into two primary components. The first is the Schilling Titan II manipulator. The second is the fixture that simulates the mating of the nozzle dam and nozzle ring.

2.1.1 Schilling Manipulator

The Field and Space Robotics Laboratory had at its disposal a Schilling Titan II six degree of freedom hydraulic manipulator (see Figure 3). This robot is widely used for remote manipulation in hostile environments such as deep-ocean, toxic-chemical, high-voltage, and radioactive environments. Electricité de France (EDF) is currently using a Schilling manipulator to attempt the nozzle dam insertion process by teleoperation. The Schilling lends itself well to the task because of its large workspace with a 1.94 m (76.3") maximum reach and its high load bearing capacity of 109 kg (240 lbs) at full extension (Tomcat Manipulator System Technical Manual, 1991).

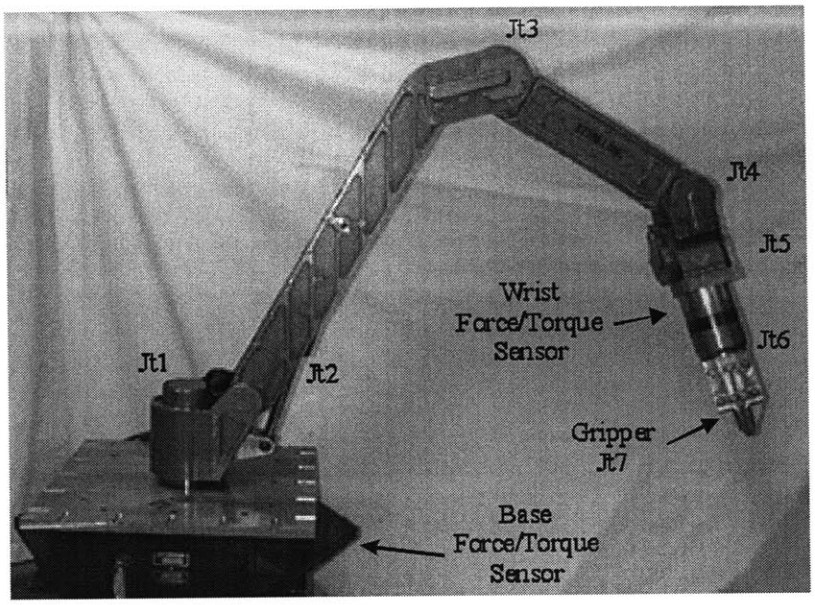

Figure 3 - Schilling Manipulator

The Schilling has six joints as well as a jaw for gripping objects in its workspace (Table 1). Each joint has a resolver containing magnetic windings which form an outer stationary ring (the stator) and an inner rotating ring (the rotor). When the resolver is excited at a particular frequency, the output changes as a function of the sine and cosine of the relative angle between the rotor and the stator. This can be used to determine joint position information. The particular resolvers in the Schilling have an accuracy of 0.7 arc minute (Tomcat Manipulator System Technical Manual, 1991).

Joint	Function	Actuator Type	Torque/Force @3000 psi	Mechanical Range	Maximum Slew Rate	Position Sensor
1	Yaw at Azimuth	Rotary vane	1600 ft-lb	270°	64°/sec	Resolver
2	Pitch at Shoulder	Linear	6500 lb	120°	64°/sec	Resolver
3	Pitch at Elbow	Rotary vane	890 ft-lb	270°	112°/sec	Resolver
4	Pitch at Wrist	Rotary vane	412 ft-lb	180°	240°/sec	Resolver
5	Yaw at Wrist	Rotary vane	412 ft-lb	180°	240°/sec	Resolver
6	Wrist Rotation	Gerotor	50 ft-lb	360° cont.	60 rpm	Resolver
7	Jaw Open/Close	Linear	300 lb	4.2 in.	4.0 in./sec	LVDT

Table 1 - Schilling Joint Information

The Schilling requires two power supplies. The primary power source is a hydraulic pump which supplies the nominal pressure of 3000 psi and the hydraulic oil

flow of 1.5 to 5 gpm required to operate the Schilling. A solenoid enables and disables the hydraulic power in the Schilling. The second power source drives a series of seven servovalves which control the flow of the hydraulic oil through the joints of the manipulator.

The manipulator itself contains a six degree of freedom wrist force/torque sensor which uses strain gauge transducers to measure forces exerted on or by the Schilling end-effector. In addition, the Schilling was mounted on a six-axis Advanced Mechanical Technology, Inc. (AMTI) force/torque sensor (AMTI, 1991). The base sensor reflects dynamic and gravitational effects of the entire manipulator, while the wrist sensor is only influenced by the end-effector contact forces and payload inertial and gravitational forces (Gorinevsky, 1998). As will be discussed later, information from both sensors prove useful for the nozzle dam task.

2.1.2 Nozzle Dam and Nozzle Ring

While the FSRL had a manipulator which lent itself to the nozzle dam insertion task, a mechanical system had to be designed to emulate the nozzle dam and nozzle ring.

Based on technical drawings provided by Dr. Byung-Hak Cho, a visiting scientist from the Korea Electric Power Research Institute (KEPRI), the actual nozzle dam was realized in a foam model (Figure 4b). This allowed the problem to be fully understood before progressing with the design of the experimental system. The nozzle dam is a heavy (70 kg) object composed of two parts. A folding outer section (35 kg) secures to the meter in diameter nozzle ring by bolts, and a center plate (35kg) is then anchored to the folding section to completely seal the opening. There are two reasons for the division of the nozzle dam into sections. First, the steam generator access portal is 40 cm in

diameter requiring the nozzle dam fold in order to be passed into the chamber. Second, as one unit, the weight of the nozzle dam would be unmanageable by a human operator.

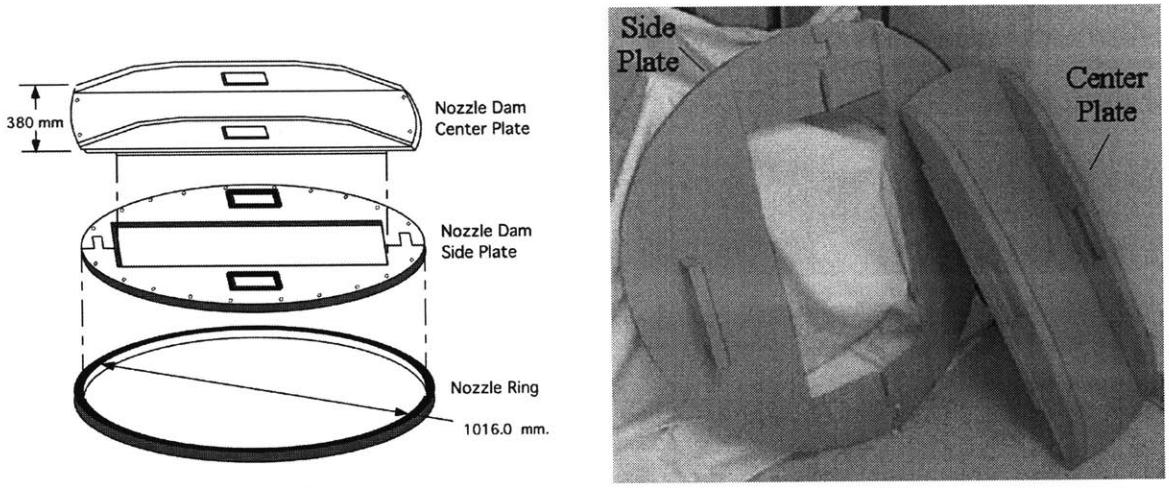

(a) (b)

Figure 4 –Nozzle Dam Drawing (a) and 1:1 Scale Foam Model (b) of Nozzle Dam

The insertion of the center plate within the side plate was determined to be a representative problem for the nozzle dam task. For the insertion to be successful, the center plate would have to be manipulated in all six degrees of freedom to within the mating tolerances. It was decided that a variable tolerance fit was to be designed. This allows for the evaluation of control algorithms as applied to various acceptable positioning errors. The system was designed to allow fits ranging from interference to a few centimeters.

To generate a fit with sub-millimeter tolerances over a 1016 mm (40") global mating edge, the variation in the individual pieces must be very small. A large 1016 mm x 381 mm x 12.7 mm (40"x15"x0.5") piece of aluminum was machined to tolerances of a few thousandths of an inch. This was necessary since the tolerance of the saw cut on the aluminum stock was 1.59 mm (0.0625").

To allow the Schilling to manipulate the massive insertion plate, a gripper had to be designed and constructed. A prototype handle had been built which closely matched the anatomy of the Schilling gripper (Figure 5). The handle was welded to increase its durability and to reduce deflections. It was then bolted to one side of the aluminum center plate providing a repeatable grip for the manipulator.

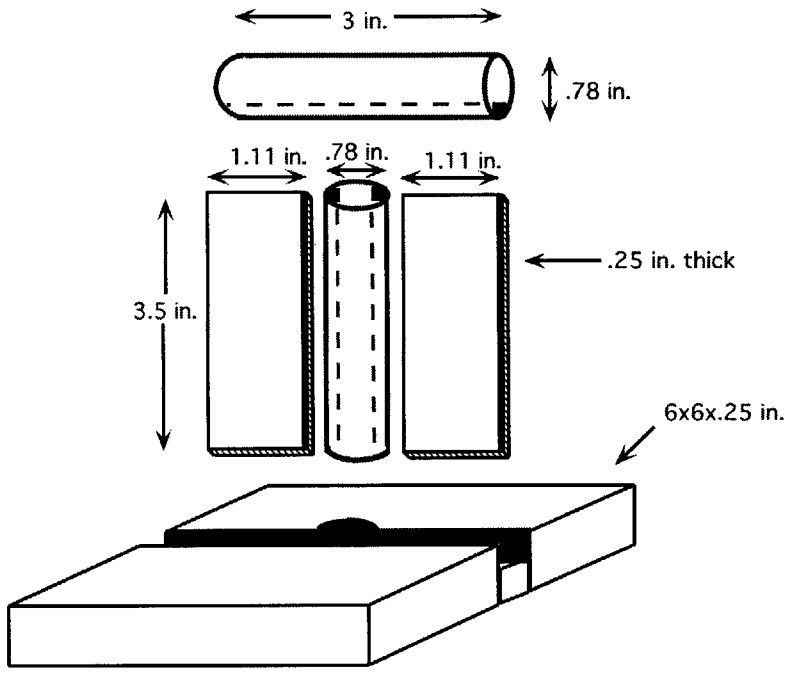

Figure 5 – Insertion Plate Handle

The use of extruded aluminum square tubing to construct the remaining mating surfaces reduced the design difficulty and cost since the surface variation of standard aluminum square tube stock was within acceptable levels. A 1016 mm (40") tube was laid on a marble table, and height measurements were made along its length. This confirmed maximum variations of 0.05 mm (0.002") along any of the four sides. Therefore, aluminum tubing was bolted to the other side of the aluminum plate to form the lower insertion plane boundaries. The receptacle was built by anchoring additional tubing to a fixed aluminum plate creating boundaries that would mate with the insertion

plate. On two adjacent sides, inner rails were mounted on bolts to allow adjustment of their positions with respect to the fixed outer rails. By modifying the adjustment bolts on the two edges, the mating tolerances can be set arbitrarily. The design schematics are shown in Figure 6.

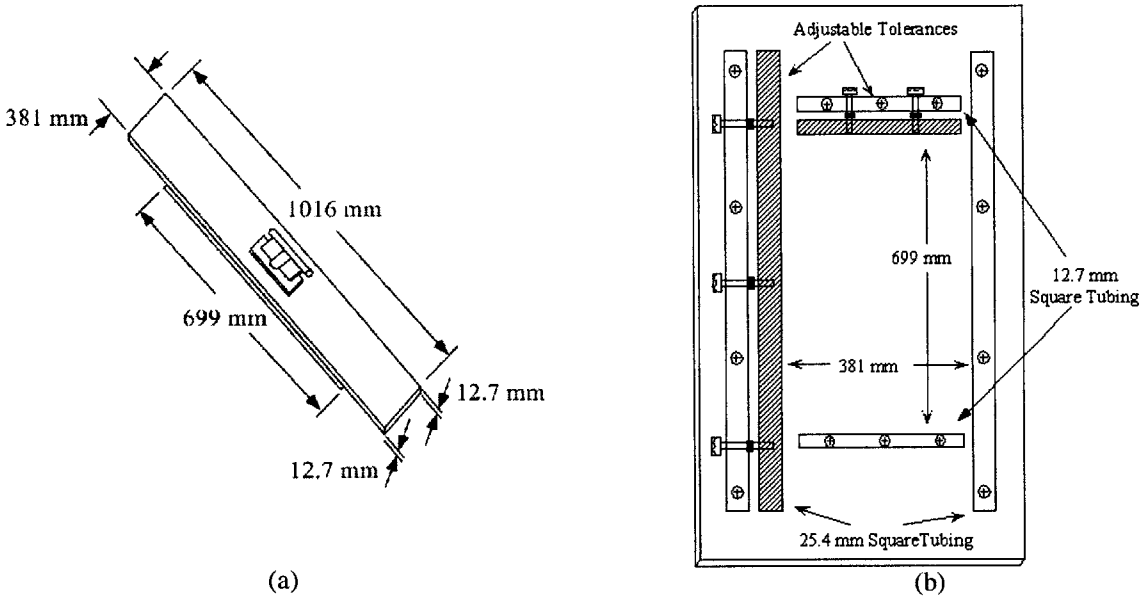

Figure 6 - Nozzle Dam Center Plate (a) and Variable Tolerance Receptacle (b)

Once the insertion plate and receptacle were built, they had to be mounted in the workspace. The mounting structure was built from 38.1 mm (1.5") angle iron, and it supports the receptacle so that the working configuration of the manipulator is representative of the actual task. Cross-bracing and 6.35 mm (¼") hex bolts with lock washers allow the structure to withstand all expected forces imposed by the Schilling without significant deflections. Figure 7 shows an isometric drawing of the mounting design.

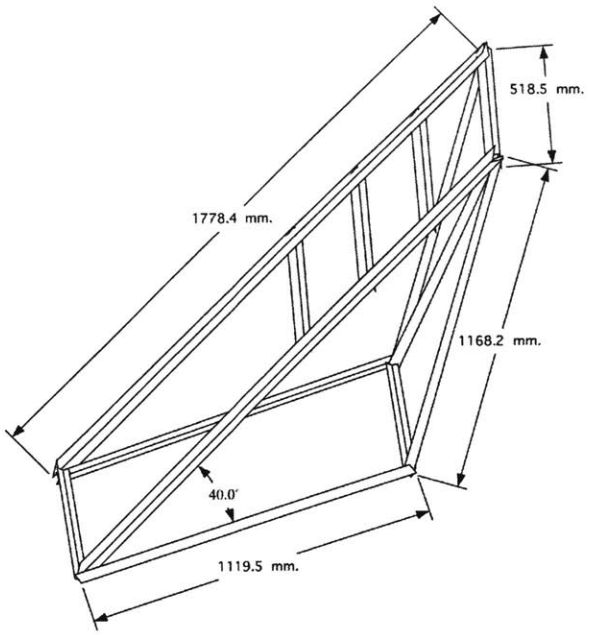

Figure 7– Isometric of the Mounting

Figure 8 shows the resulting 18 kg (39.6 lbs) insertion plate set within the variable tolerance receptacle which is mounted in the workspace of the Schilling.

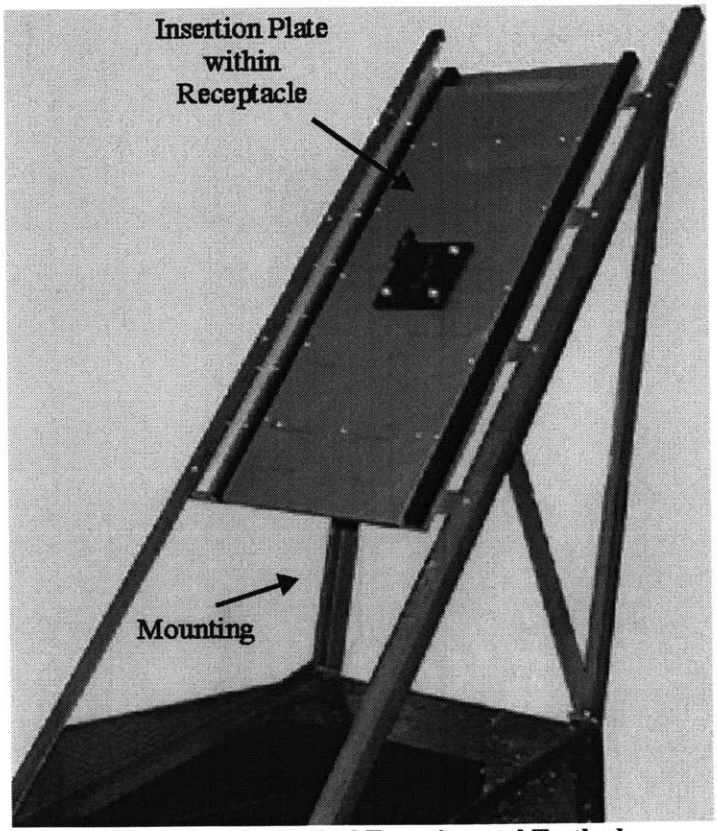

Figure 8 – Mechanical Experimental Testbed

2.2 Electrical System

The original control electronics for the Schilling manipulator is a VMEbus system designed to be a universal robot controller. The system involves multiple processors and I/O boards. The system has been applied to a Puma electric manipulator, a six degree of freedom Stewart Platform, and a wall climber referred to as Libra. However, this system proved inadequate to fully explore the nozzle dam task. Therefore, the system was modified to extend its capabilities.

2.2.1 Original Electronics

The universal robot controller is comprised of a VMEbus and a Sun 3/80 Workstation. The VMEbus contains, in ascending slot order:

- Motorola 68030 processor with a Floating Point Unit and Ethernet card
- Motorola 68020 processor
- Delta Tau Data Programmable Multi-Axis Controller (PMAC)
- Data Translation 16-bit ADC and 12-bit DAC
- Custom VMEbus interface for the Stewart Platform leg controllers

The VME processors run the real-time operating system (OS) VxWorks, version 4.0.2 (Wind River Systems, 1991). Upon power up, the 68030 processor, the system controller since it resides in slot 1, has an EPROM that bootstraps the system and downloads an image of the VxWorks OS from the Sun workstation via the Ethernet link. The processor establishes a heartbeat on the bus to signal other processors that the backplane is active. The second processor can then access the Ethernet card, and download a VxWorks image to boot itself. Application code is created on the Sun workstation and compiled using a VxWorks compiler. The executable is then

downloaded to the VME processor where it is run. The processor can then interface to other VME cards while running the desired control loop.

The PMAC installed in this system is a VMEbus eight-axis industrial motion control card. It has A QUAD B and C encoder inputs, 16-bit analog outputs, digital I/O and an on board DSP capable of handling up to 56-bit computations. It can perform individual servo PID loops in 60 μs (PMAC User's Manual, 1992). Commands can be passed to the PMAC over the VMEbus by writing to its mailbox. This is a slow process that involves writing an ASCII command in 15-byte blocks. This method is adequate for establishing initial configurations and passing non time-critical commands. Dual port rapid access RAM (DPRAM) was added to the PMAC to allow high-speed read and writes over the VMEbus which allow for data passing during active control. The VMEbus and Sun workstation reside in a control room as designated in Figure 9.

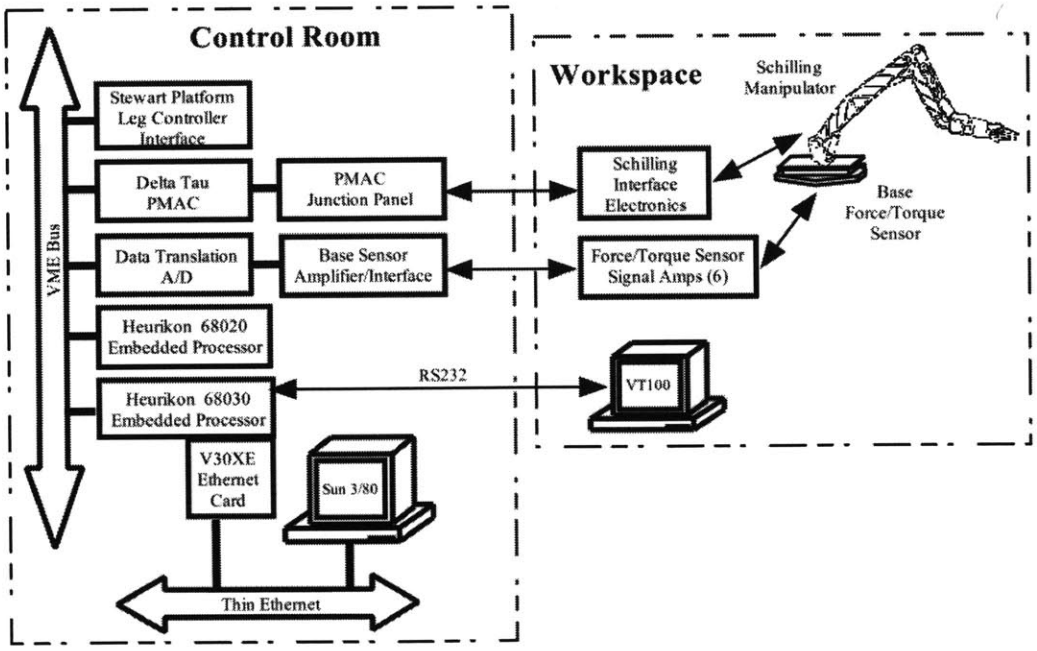

Figure 9 - Original Electrical System

To control a specific robot, the correct connections must be established as shown by the lines linking the workspace and control room in Figure 9. The desired robot's interface cable is plugged into the custom 25 pin connector on the PMAC junction panel. The junction panel has a port for each of the PMAC's 8 channels, as well as a custom port which provides 7 channels of encoder inputs and DAC outputs as well as digital inputs for positive and negative limit switches. If a base sensor is going to be used, the output of the desired sensor amplifier/interface unit must be connected to the first 8 channels of the Data Translation 16 channel differential ADC card. The first six channels are used and the 7^{th} and 8^{th} are tied to ground since floating channels can induce noise on nearby channels. Given that the interface electronics for the individual robot is powered, applications running on the VME processors can now control the desired robot.

The PMAC is also used to interpret position information from the Schilling manipulator. However, the joint resolver signals must be converted to quadrature encoder signals in order to be compatible with the PMAC. A Delta Tau Data 12-bit resolver to digital converter board accomplishes this task, achieving joint angle resolution of ±0.087 degrees. A 0.087 degree error in the first joint corresponds to a 3 mm (0.12") error in the end-effector position when the Schilling is at full extension. Undetectable displacements in all of the joints could lead to end-point position errors of 5 mm (0.20"). This may prevent the current configuration of the Schilling system from achieving an actual nozzle dam placement since the mating tolerances are on the order of 1 mm. However, this limitation doesn't prohibit conducting considerable research in the field since the variable tolerance receptacle allows investigating tolerances both below and above the joint position resolution.

The Schilling power stage must allow the PMAC's DAC output to control the joints of the manipulator. The servovalves are current controlled and only require peak currents of 8 mA. This allowed the use of standard op-amps to implement the power stage to scale ±10 V signals from the DAC to ±8 mA drive currents: a gain of $8 \cdot 10^{-4}$ (Figure 10).

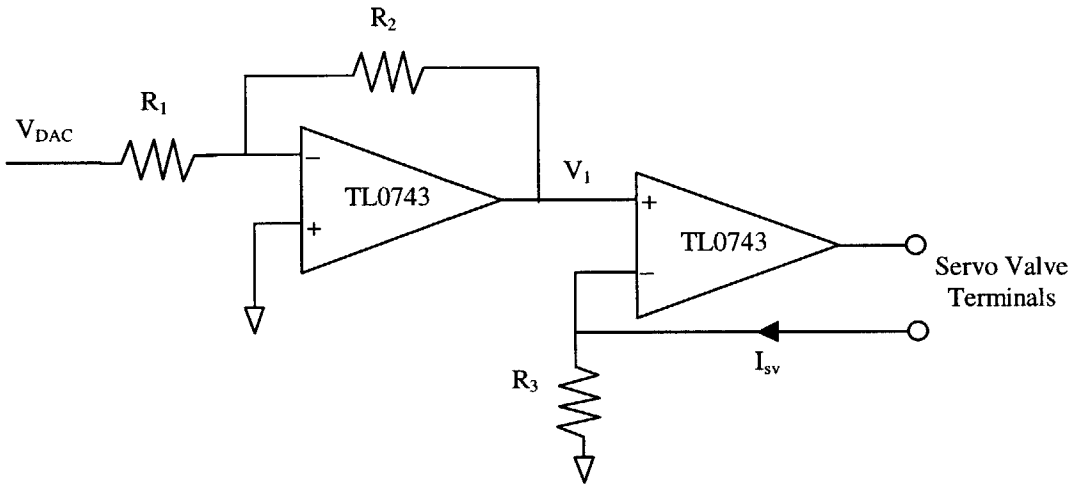

Figure 10 - Current Controlled Power Amp

The relation between V_{DAC} and I_{sv} becomes:

$$I_{sv} = \frac{V_1}{R_3} = -\frac{R_2}{R_1 R_3} V_{DAC} \qquad (2\text{-}1)$$

Reasonable resistor values were chosen to be R_1=100 kΩ, R_2=39 kΩ, and R_3=470 Ω. These result in a scaling factor of $8.30 \cdot 10^{-4}$. Additional circuitry included a relay and digital logic allowing a button box to activate the Schilling's solenoid to enable or disable hydraulic power.

The PMAC is actively used in one of two modes. First, it can function as an eight axis PID servo controller where gains are initially set and motions are generated by discrete displacement commands passed to the PMAC mailbox. The PMAC code "#3"

would select joint 3 and "J=276" would move that joint to encoder position 276. PMAC variables determine the shape of the trajectories that will be generated. However, custom control algorithms can be implemented using the 68030 processor and switching the PMAC into its alternate mode.

The second functional mode requires the creation and activation of a PMAC PLC program. These programs are referred to as PLCs because of their functional similarity to hardware programmable logic controllers. By scripting a PLC to copy a block of DPRAM into its DAC registers, values written to that specific DPRAM block over the VMEbus end up specifying the command outputs of the PMAC. The PMAC can support up to 32 of these programs which continually run in background. PLCs can be interrupted by motor commutation, servo loop closure, move planning, or PLC 0. Since the servo loops are disabled in this mode and PLC 0 is not active, the memory transfer operates at frequencies well above the sample rate of any practical custom control loop. In order for the 68030 to calculate command values, it needs to get position feedback from the Schilling. This is provided by a second PLC which continually copies the PMAC's encoder registers to another DPRAM block. The processor reads that DPRAM block over the VMEbus to acquire the most recent position data. Using the DPRAM as an intermediary between the 68030 and the PMAC DAC and encoder registers, custom position control loops can be run on the processor.

Force information is also available to the 68030 processor. The processor can initiate an analog to digital conversion by the Data Translation board. The processor writes the desired starting (1) and ending (6) channels to a register in the ADC. It then writes an additional register to begin the conversion. The processor continually polls the

ADC board reading each channel of the AMTI force/torque sensor as they are sampled. This information is useful for the custom control algorithms discussed in Section 3.2.

The control electronics described above were functional, but presented significant limitations that impeded researching the nozzle dam insertion problem. The current control algorithms were already pushing the computation power boundary of the 20 MHz Motorola 68030. This was apparent since the sample period was almost entirely occupied with computation time. The user interface also posed significant limitations since it was a VT100 terminal using an RS-232 interface. A sequence of actions was given discretely with a finite set of data displayed between commands. A discrete, text-based controller is a difficult environment in which to explore automation of the nozzle dam task. In addition, modifications to the code were made using a text editor on the Sun workstation in the adjoining control room. The compiler had limited debugging tools, and the process of compiling and loading new executables was time consuming and made even minor changes a substantial time sink. These limitations led to the need for a modified control system. However, the new system should interface with the legacy system to maintain support for the universal robot controller.

2.2.2 Modified Control System

The modified control system augments three aspects of the original system: computation power, the user interface, and environmental contact sensing capabilities. The corner stone of this implementation was the acquisition of a 300 MHz PC.

An Ultralink PC VME link interface was added to phase the PC into the VMEbus Schilling control system. This included adding both a VME link card to the VMEbus and an ISA link card to the PC. This allows an application written in any PC programming

language to access the VMEbus through reads and writes to the PC's I/O ports. The VME link was configured to provide the PC with the same functionality as any other processor on the VMEbus. If the VMEbus is unoccupied when the PC requests the bus, the system controller's arbiter grants the VME link the bus by activating a bus grant signal (BGR) which is passed up the VME backplane. However, to prevent a race condition when multiple processors simultaneously request the bus, the bus grant signal is daisy chained through each card ensuring that only the first processor requesting the bus receives the signal (VMEbus User's Handbook, 1988). Since the eight-axis PMAC occupies one and a half VME slots, jumpers were installed in the VME backplane to extend the bus grant chain beyond the slot occupied by the additional four-axis PMAC control card. Jumpers had already been installed to bypass the Ethernet card which occupies a half slot above the 68030 processor. The newly placed jumpers allow the VME link card to receive bus grant signals in response to its requests. Upon receiving a bus grant, the VME link has established a buslink. After writing a VME address to specific PC I/O ports, data can be either read from or written to the VME shared memory address space.

Driver code was written to provide a layer of abstraction for PC I/O port level commands that initialize the PC VME link as well as perform the VMEbus reads and writes (see Appendix A.1 for function prototypes). The VMEbus is a versatile architecture which allows 16-bit, 24-bit, or 32-bit address spaces with 8-bit, 16-bit, or 32-bit data words. The PC VME Link has capabilities for up to 24-bit address space and 16-bit data. However, the Data Translation card uses the 16-bit address space while the PMAC uses the 24-bit address space. Both cards do use 16-bit data words. Therefore

provisions were made in the read and write procedures to allow designation of the different address spaces. A single 16-bit data transfer between the PC and the PMAC's DPRAM was demonstrated to be on the order of 10 μs. Therefore, 100 data transfers would occupy less than 10% of a 10 ms sample period. Since less than 50 transfers are expected, this interface allows the PC's input/output capabilities to match those of the 68030 processor while greatly expanding the computation power.

The new PC presented the opportunity for selecting a new software development environment. Turbo C++ was chosen as the compiler since a graphical simulation was already under development in that environment (see Chapter 4). Turbo C++ was also being used for other real-time control applications in the laboratory. However, to perform real-time control on the PC, a method of generating real-time interrupts was required. An ISA counter/timer card was acquired and installed in the PC (NuDAQ, 1996). Software was written to generate interrupts (IRQ7). The timer card has a 2 MHz clock which is frequency divided by two staged 16-bit counters. The first counter was set to the fixed value 1000 to divide the clock frequency to 2 kHz. This allows the second counter to specify sample periods shorter than 1 ms and as long as 32 seconds. An Interrupt Service Routine (ISR) was written to handle time-critical control computations. Overall, the new computer system allowed for greater customization of the user interface, and drastically increased computation power.

The final addition to the electronics was an interface to the Schilling's internal wrist force/torque sensor. The Schilling Titan II was released in 1991, and the JR3 force/torque sensor included in the design predated 1991 and was an analog sensor using four strain gauge bridges. Each of the four bridges generates a horizontal and vertical

signal proportional to the forces and moments in the x, y, and z-axis. Based on experiments with the wrist sensor and a schematic acquired from Schilling (Figure 11), each force and torque component could be mapped to a combination of specific signals. For example, a force in the z-axis would generate signals in the vertical strain gauges, but not the horizontal; while a moment about the z axis would be reflected in all the horizontal strain gauges and none of the vertical.

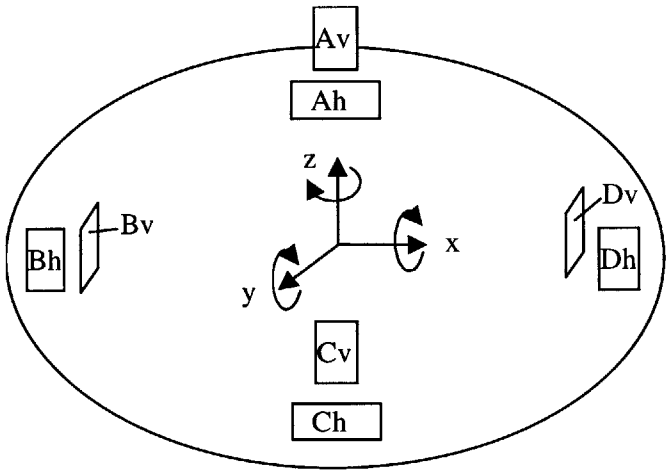

Figure 11 - Wrist Sensor Strain Gauge Configuration

The millivolt-level signals are amplified within the body of the Schilling manipulator (Tomcat Manipulator System, Technical Manual, 1991). The sensor had not been previously wired and no calibration data was available. The relations between the strain gauge signals and the force components are shown in Equation (2-2). Experiments were designed to determine the full calibration matrix since coupling between force components was apparent.

$$\mathbf{C}_{6x6} \cdot \begin{bmatrix} Ch - Ah \\ Bh - Dh \\ Av + Bv + Cv + Dv \\ Av - Cv \\ Dv - Bv \\ Ah + Bh + Ch + Dh \end{bmatrix} = \begin{bmatrix} F_x \\ F_y \\ F_z \\ \tau_x \\ \tau_y \\ \tau_z \end{bmatrix} \tag{2-2}$$

To determine the calibration matrix, various masses were hung at specific points on the end-effector creating a known set of forces and moments. Output voltages were measured, and matrices $\hat{\mathbf{V}}$ and $\hat{\mathbf{F}}$ were constructed and contained a set of experimentally measured voltages and matching ideal forces respectively.

$$\mathbf{C} \cdot \hat{\mathbf{V}} = \hat{\mathbf{F}} \tag{2-3}$$

The calibration matrix was found by using Matlab to evaluate the pseudoinverse as shown in Equation (2-4).

$$\mathbf{C} = \hat{\mathbf{F}} \cdot (\hat{\mathbf{V}}^T \cdot \hat{\mathbf{V}})^{-1} \cdot \hat{\mathbf{V}}^T \tag{2-4}$$

Figure 12 shows a histogram of 1,000 readings of the unloaded wrist sensor (forces are measured in newtons and torques in newton·meters). The distribution shows the sensor has a considerable amount of noise which was experimentally found to be in the form of a Gaussian distribution. Fortunately, the mean values were observed to be relatively accurate.

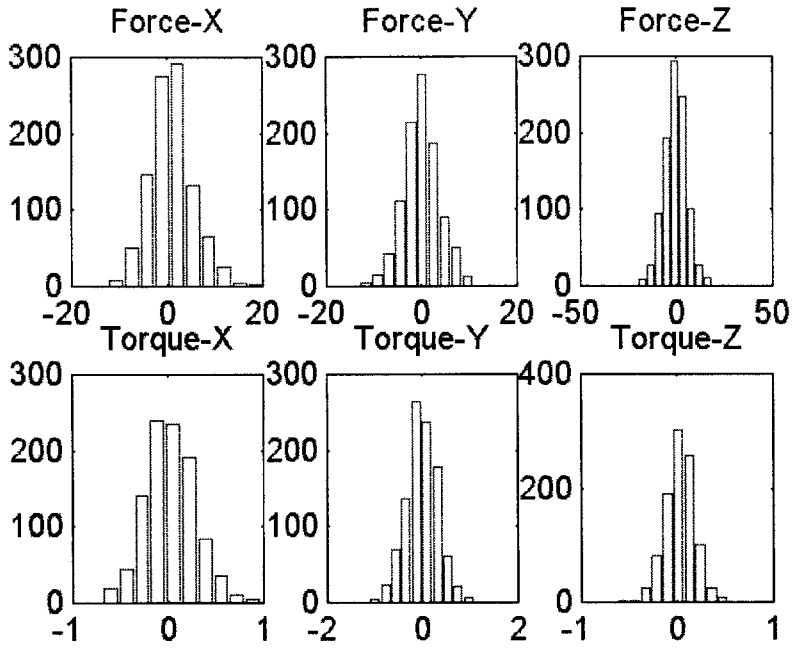

Figure 12 - Histogram of Wrist Sensor Noise (forces [N] and torques [Nm])

The mean values and standard deviations of each channel were computed (see Table 2).

	Fx [N]	Fy [N]	Fz [N]	τ_x [Nm]	τ_y [Nm]	τ_z [Nm]
Mean	1.0025	0.0915	-0.2593	0.0189	-0.0154	0.0231
Standard Deviation	4.5381	3.6699	5.9396	0.2637	0.3328	0.1568

Table 2 - Noise Parameters of Wrist Force/Torque Sensor

The wrist sensor must also be zeroed to establish a reference state. This requires reading the sensor several times initially without a payload on the end-effector. These values are averaged in order to extract the mean value from the Gaussian distribution, and the mean values become the offset force vector. Future readings are also averaged to reduce noise, and the offset vector is subtracted to determine the forces imposed on the end-effector with respect to the zero-load state.

The new electrical system (Figure 13) added considerable capabilities in the forms of computation power, the potential for a graphical user interface, and the ability to

measure contact forces with the wrist force/torque sensor. The current system still requires the 68030 processor to release control of the Schilling to the PC. This is necessary because the PMAC mailbox communication protocol has yet to be ported to the PC. Such an implementation would require the PC VME interface to be configured to service VMEbus interrupt 4. Currently, the 68030 need only set up and activate the necessary PMAC PLCs linking specific blocks of the PMAC's DPRAM with the encoder and DAC registers as described in Section 2.2.1.

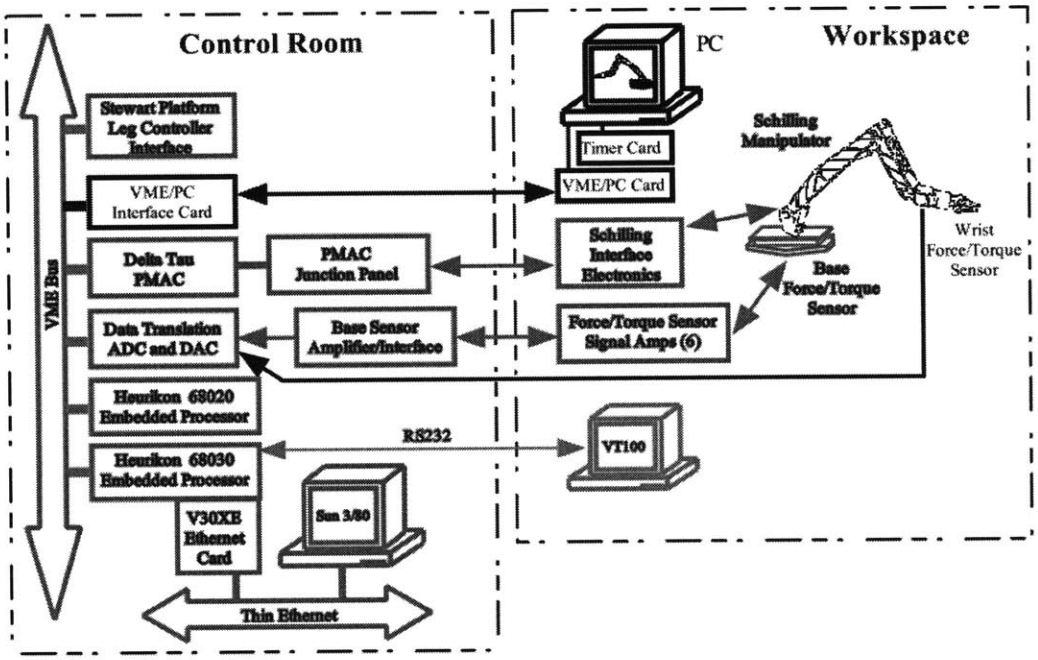

Figure 13 - Modified Electrical System

Chapter 3

High Precision Manipulator Control

3.1 Background

The nozzle dam insertion task requires the use of a robust and strong manipulator to manage the heavy nozzle dam payload within the harsh radioactive environment of the steam generator. However, typical of strong, powerful manipulators, the Schilling does not inherently have fine repeatability due to high joint friction. Also, absolute accuracy is sacrificed as a result of the poor repeatability and significant geometric and elastic errors. Yet, the nozzle dam task requires extremely accurate positioning for fine motions. The objective is to achieve high performance for small motions while minimizing the implementation cost to keep the solution practical for the nuclear industry.

In this research, an approach is presented that substantially improves the absolute accuracy of the Schilling manipulator. The Base Sensor Control (BSC) method uses base force/torque sensor information to improve manipulator repeatability (Morel, 1996). This is applied in concert with a Geometric and Elastic Error Correction (GEC) algorithm which uses offline calibration data and real-time wrist sensor information to achieve greatly improved absolute accuracy in a strong manipulator exerting high task loads (Meggiolaro, 1998). The effectiveness of this solution is shown experimentally on the Schilling hydraulic manipulator. The combined method does not require joint velocity or acceleration measurements, a model of the actuators or friction, or the knowledge of manipulator mass parameters or link stiffness. Yet, it is able to substantially improve absolute positioning accuracy of the manipulator.

3.2 Base Sensor Control (BSC)

A number of approaches exist for improving fine motion manipulator repeatability performance through friction compensation. Some of these require modeling of the difficult to characterize joint frictional behavior (Canudas-de-Wit, 1996; Habibi, 1994; Merritt, 1967; Popovic, 1994). Some require the use of specially designed manipulators that contain complex internal joint-torque sensors (Pfeffer, 1989).

A simple, yet effective control method has been developed that is model-free and does not require internal joint sensors (Morel, 1996). The method, called Base Sensor Control (BSC), estimates manipulator joint torques from a self-contained external six-axis force/torque sensor placed under the manipulator's base. The joint torque estimates allow for accurate joint torque control that has been shown to greatly improve repeatability of both hydraulic and electric manipulators (Iagnemma, 1997).

3.2.1 BSC Theory

The following is a brief review of the basis for BSC summarized from the complete development presented in (Morel, 1996). A simplified version of the algorithm sufficient and effective for fine-motion control is formulated in (Iagnemma, 1997).

As shown in Figure 14, the wrench, $\mathbf{W_b}$, exerted by the manipulator on its base sensor can be expressed as the sum of three components:

$$\mathbf{W_b} = \mathbf{W_g} + \mathbf{W_d} + \mathbf{W_e} \tag{3-5}$$

where $\mathbf{W_g}$ is the robot gravity component, $\mathbf{W_d}$ is caused by manipulator motion, and $\mathbf{W_e}$ is the wrench exerted by the payload on the end-effector. Note that joint friction does not appear in the measured base sensor wrench. In the fine-motion case, it is assumed that the gravity wrench is essentially constant, and this wrench can be approximated by an

initial value measured by the base sensor. Hence, the complexity of computing the gravitational wrench, such as identification of link weights and a static manipulator model, is eliminated. Under this assumption, the Newton Euler equations of the first i links are:

$$\begin{cases} \mathbf{W}_{0\to 1} = -\mathbf{W}_b \\ \mathbf{W}_{1\to 2} = \mathbf{W}_{0\to 1} - \mathbf{W}_{d_1} \\ \vdots \\ \mathbf{W}_{i\to i+1} = \mathbf{W}_{i-1\to i} - \mathbf{W}_{d_i} \\ \vdots \\ -\mathbf{W}_e = \mathbf{W}_{n-1\to n} - \mathbf{W}_{d_n} \end{cases} \tag{3-6}$$

where $\mathbf{W}_{i\to i+1}$ is the wrench exerted by link i on link i+1, and $\mathbf{W}_{d_i}$ is the dynamic wrench for link i.

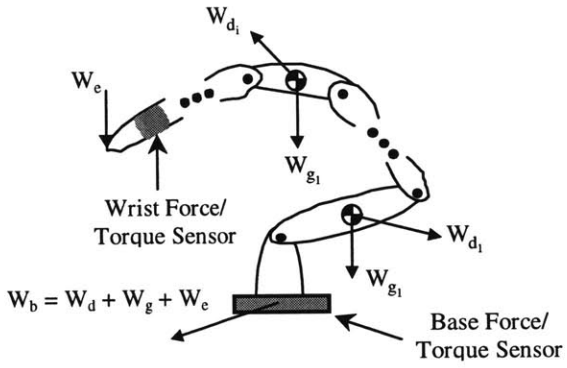

Figure 14 - Manipulator External and Dynamic Wrenches (Morel, 1996)

For fine tasks it is assumed that the manipulator moves very slowly so that $\mathbf{W_d}$ can be neglected. Therefore, for slow, fine motions, only the measured wrench at the base is used to estimate the torque in joint i+1. The estimated torque in joint i+1 is obtained by projecting the moment vector at the origin O_i of the i^{th} reference frame along the joint axis z_i:

$$\tau_{i+1} = -z_i^{\,T} \cdot \mathbf{W}_b^{\,O_i} \tag{3-7}$$

The value of τ_{i+1} depends only on joint positions, the manipulator's kinematic parameters and the base sensor measurements.

With estimates of the joint torque, it is possible to perform high performance torque control that can greatly reduce the effects of joint friction and nonlinearities. Figure 15 shows an application of BSC to a typical manipulator. The result of this control loop is greatly improved manipulator repeatability.

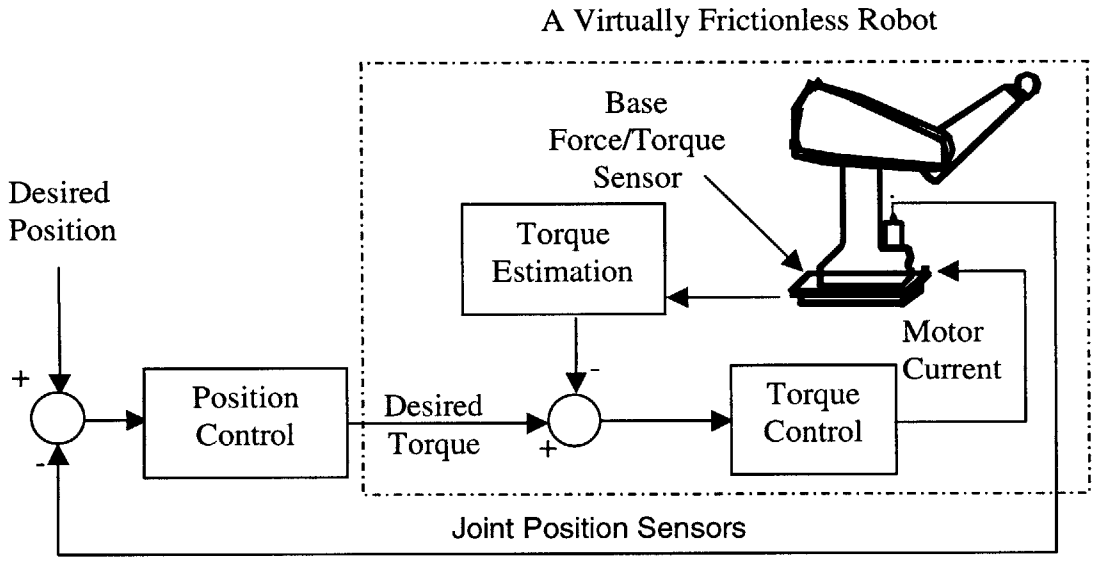

Figure 15 - BSC Control Loop (Morel, 1996)

However, The BSC method does not compensate for sources of random repeatability errors, such as limited encoder resolution. In addition, a manipulator with high repeatability does not necessarily have fine absolute position accuracy.

3.2.2 BSC Experimental Data

The objective of the experiment was to see if the method outlined in Figure 15 could be applied to the Schilling experimental system to improve its repeatability. The Schilling was commanded to a particular joint space configuration where the tip of a pencil lightly touched a sheet of poster board fixed in the workspace. The Schilling was

then moved to an arbitrary point in joint space and commanded to return to the initial joint configuration. The root mean square error of the resulting points was used as a measure of the system repeatability. The object was to have the residual error of this experiment approach the limit set by the position sensing resolution of the system.

Measurements of the manipulator under PI control were taken to determine the baseline uncompensated system repeatability. Recall that the 12-bit discretization of the resolver signal leads to random errors up to 5.0 mm (see Section 2.2.1), and imposes a lower limit of approximately 2.0 mm (RMS) on the system repeatability as determined by evaluation of the Schilling's workspace and joint angle resolution. These values represent the accuracy limit of any error compensation algorithm since position variations within these values may not be detectable.

Figure 16 shows the distribution of the repeatability error with and without BSC. The results show that implementing the BSC algorithm reduced the repeatability errors by a factor of 4.73 over PI control. The initial position to which the Schilling was continually commanded bears the label "Reference Position." The maximum magnitude error without BSC was 21.0 mm, and the repeatability was 14.3 mm (RMS). BSC reduced the maximum magnitude error to 5.5 mm with a repeatability of only 3.0 mm (RMS).

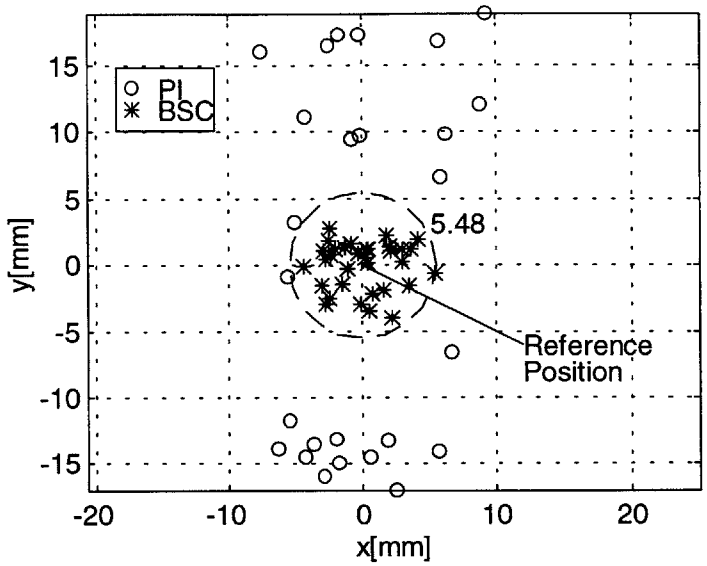

Figure 16 - Repeatability with and without BSC

Although the BSC algorithm greatly reduced the repeatability errors, what is not apparent from the results shown in Figure 16 is that a 35 mm (RMS) error in absolute accuracy remains.

Even with improved repeatability, high absolute positioning accuracy is still difficult to achieve with a strong manipulator. Non-ideal geometry of the links and joints of the manipulator create kinematic errors which contribute to poor absolute accuracy. Task constraints often make it impossible to use direct end-point sensing to compensate for these errors. Therefore, there is a need for model-based error identification. With the system repeatability reduced to 3.0 mm by BSC, a model based error correction method described below can be applied to reduce the accuracy errors to a similar level.

3.3 Geometric and Elastic Error Compensation (GEC)

Considerable research has been done in the area of model based error correction, commonly referred to as robot calibration (Hollerbach, 1988; Roth, 1986). These methods attempt to correct for geometric errors resulting from non-ideal contributions to

the kinematics of a manipulator. Often, an additional error source can also limit the absolute accuracy of a large manipulator. Powerful manipulators are designed to manage heavy payloads, however they can still be subject to elastic errors due to the distortion of a manipulator's mechanical components under large task loads. Methods have been developed to deal with this problem (Vaillancourt, 1994). These methods depend upon detailed and difficult to obtain analytical models of the manipulator.

Recent work has resulted in a method that can correct for errors in the end-effector position and orientation caused by geometric and elastic errors in large manipulators (Drouet 1998; Meggiolaro, 1998). The method, called Geometric and Elastic Error Compensation (GEC), is a measurement based error compensation algorithms that predicts the manipulator's end-point position and orientation as a function of the configuration of the system and the task forces. Given the task loads from a conventional wrist force/torque sensor and the joint angles of the manipulator, the algorithm compensates for the combined elastic and geometric errors. It does not require detailed modeling of the manipulator's structural properties. Instead it uses a relatively small set of offline end-point experimental measurements to build a "generalized error" representation of the system (Mavroidis, 1997). It has been shown that these methods can substantially reduce the absolute errors in manipulators with good inherent repeatability.

3.3.1 GEC Theory

The main sources of absolute accuracy errors in a manipulator with good repeatability are mechanical system errors (resulting from machining and assembly tolerances), elastic deformations of the manipulator links, and joint errors (such as

bearing run-out). These can be grouped into geometric and elastic errors. Although these physical errors are relatively small, their influence on the end-effector position of a large manipulator can be significant. Presented below is a brief review of the error compensation method implemented in this work (Meggiolaro, 1998).

The end-effector position and orientation error, $\Delta\mathbf{X}$, is defined as the 6x1 vector that represents the difference between the true position and orientation of the end-effector and the ideal or desired one:

$$\Delta\mathbf{X} = \mathbf{X}^{\mathbf{r}} - \mathbf{X}^{\mathbf{i}} \tag{3-8}$$

where $\mathbf{X}^{\mathbf{r}}$ and $\mathbf{X}^{\mathbf{i}}$ are 6x1 vectors composed of the three positions and three orientations of the end-effector reference frame in the inertial reference system for the real and ideal cases respectively.

The error compensation method assumes that physical errors slightly displace manipulator joint frames from their expected, ideal locations (Meggiolaro, 1998). The real, or actual, position and orientation of each frame with respect to its ideal location is represented by three consecutive rotations and three translational coordinates. These 6 parameters are called here "generalized error" parameters. For an n^{th} degree of freedom manipulator, there are 6n generalized errors which can be represented by a vector ε.

When the generalized errors are included in the model, the six coordinates of the real end-effector position vector $\mathbf{X}^{\mathbf{r}}$ can be written in a general form:

$$\mathbf{X}^{\mathbf{r}} = \mathbf{f}^{\mathbf{r}}(\mathbf{q}, \varepsilon, \mathbf{s}) \tag{3-9}$$

where $\mathbf{f}^{\mathbf{r}}$ is a non-linear vector function of the configuration parameters $\mathbf{q}$, the generalized errors ε, and the structural parameters $\mathbf{s}$. In general, the generalized errors depend on the manipulator configuration $\mathbf{q}$ and the end-effector wrench $\mathbf{W}_e$, or $\varepsilon(\mathbf{q}, \mathbf{W}_e)$. To predict the

behavior of the manipulator in a given configuration, the task wrench is also used to calculate the generalized errors from previous offline measurements. For simplicity, the i^{th} element of vector ε is approximated by a polynomial series expansion of the form:

$$\varepsilon_i = \sum_j \varepsilon_i^{(j)} \cdot (q_1^{a_1^{(j)}} \cdot q_2^{a_2^{(j)}} \cdot \ldots \cdot q_n^{a_n^{(j)}} \cdot w_m^{b^{(j)}}) \qquad (3\text{-}10)$$

where q_1, q_2, ..., q_n are the manipulator joint parameters, w_m is an element of the task wrench, and $\varepsilon_i^{(j)}$ are the polynomial coefficients. It has been found that improved accuracy can be obtained by using only a few terms in the above expansion. The coefficients of these $\varepsilon_i^{(j)}$ terms are constants and become the unknowns of the problem.

Since the generalized errors are small, $\Delta\mathbf{X}$ can be calculated by the following linear equation in ε:

$$\Delta\mathbf{X}(\mathbf{q}, \mathbf{W_e}) = \mathbf{J_e} \cdot \varepsilon \qquad (3\text{-}11)$$

where $\mathbf{J_e}$ is the 6x6n Jacobian matrix of the function $\mathbf{f^r}$ with respect to the elements of the generalized error vector ε. The matrix J_e depends on the system configuration, geometry, and task wrench.

Once the generalized errors, ε, are identified, the end-effector position and orientation error can be calculated using Equation (3-11). Assuming all six components of $\Delta\mathbf{X}$ can be measured for an n^{th} degree of freedom manipulator, its 6n generalized errors ε can be calculated by fully measuring vector $\Delta\mathbf{X}$ at n different configurations. To increase the accuracy of the calculated generalized errors, additional measurements are made and a least mean square procedure is used to compute ε. All repeatable errors are identified regardless of their source.

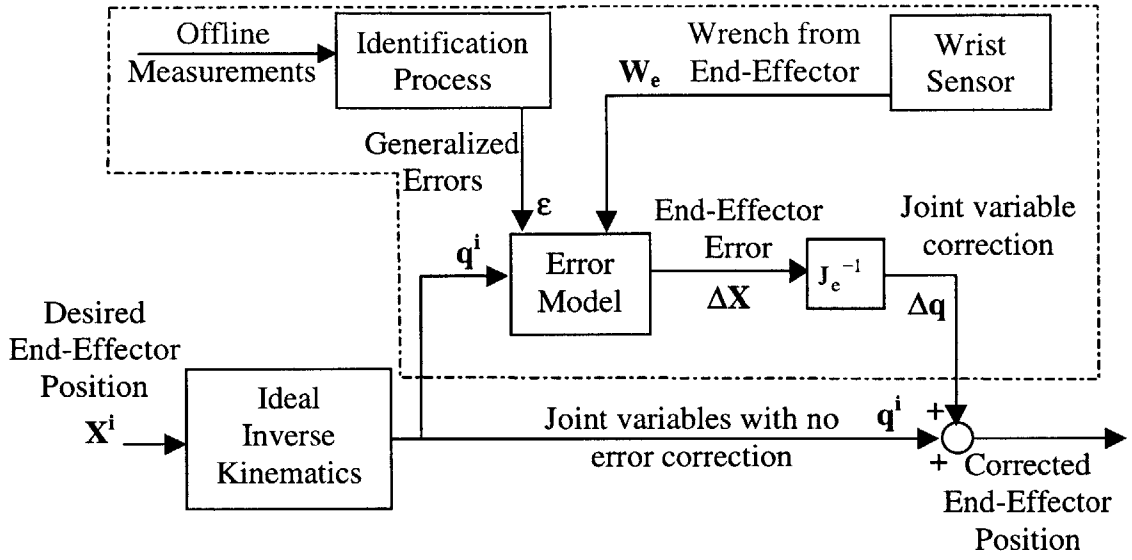

Figure 17 - GEC Control Method

Figure 17 shows how an error model of the type in Equation (3-11) can be used in an error compensation algorithm, and how the corrected joint angles can be provided to any form of joint space controller. The corrected joint angles would drive the manipulator to its actual desired end-effector position rather than the one determined by ideal inverse kinematics which might be flawed.

3.3.2 GEC Experimental Data

In this work, 400 measurements were used to evaluate the basic accuracy of the Schilling. Different payloads were used, with weights up to 45 kg. Most of the measurements focused on two specific payloads: one with no weight and another with a 18 kg weight (the replica nozzle dam plate). The measurements were taken using a pair of optical theodolites. Using these devices, the Schilling's end-effector coordinates could be triangulated in 3-D space, however this equipment could not determine orientation. The resolution of the theodolites was 30 arc seconds, which corresponded to errors of 0.29 mm for these measurements as determined by the placement of the theodolites.

End-effector measurements of the manipulator under PI control determined the baseline uncompensated system accuracy. The root mean square of the positioning error was used as a measure of the system accuracy. Recall that the system repeatability determines the lower limit of the achievable accuracy.

To implement GEC, the geometric and elastic deformation correction matrix was calculated using approximately 350 measurements of the end-effector in different configurations and with different payloads. The remaining points were used to verify the efficiency of the GEC method. Elastic errors in the Schilling due to payloads of 45 kg or less were not measurable with this equipment.

Using the Schilling's kinematic model as determined by the manipulator design schematics, the ideal coordinates of the end-effector were calculated and subtracted from the experimentally measured values to yield the vector $\Delta\mathbf{X}(\mathbf{q},\mathbf{We})$ in Equation (3-11). By treating generalized errors as constant in their respective frames, the system absolute accuracy was reduced from 35 mm (RMS) to 13.4 mm (RMS). Since the GEC method allows for the use of polynomials to describe each generalized error, a second order polynomial implementation achieved an absolute accuracy of 7.3 mm (RMS), an additional factor of 2 improvement.

Figure 18 shows the convergence of original positioning errors as large as 55.1 mm (34.3 mm RMS) to corrected errors of less than 10.7 mm (7.3 mm RMS). This demonstrates an overall factor of nearly 4.7 improvement in absolute accuracy by using the GEC algorithm.

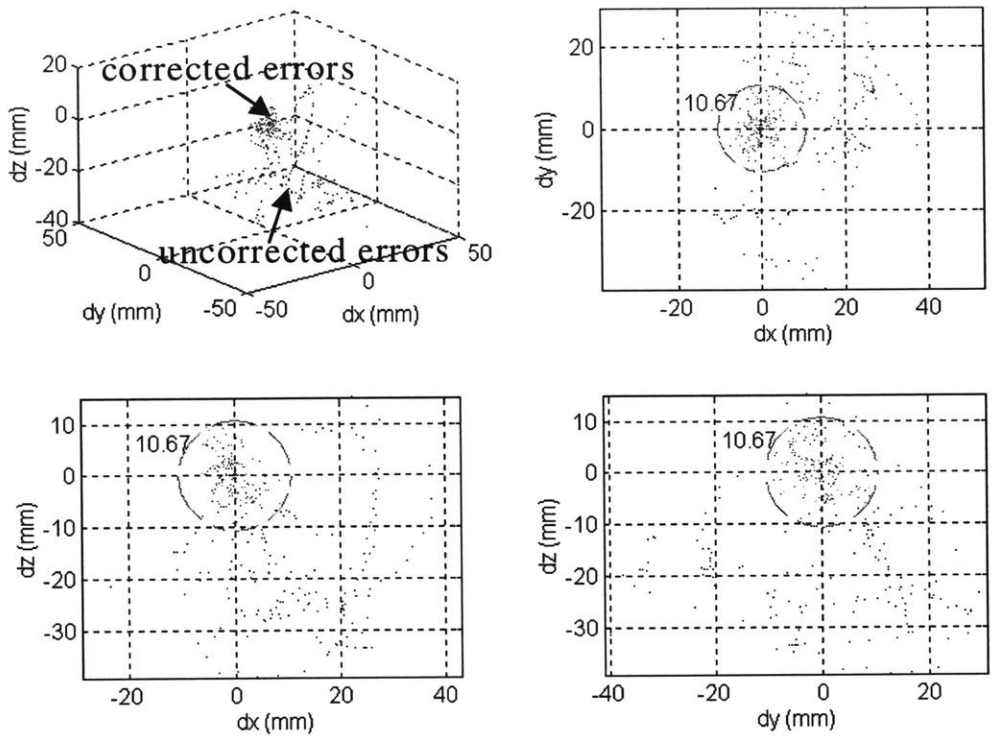

Figure 18 - Measured and Residual Errors After Compensation

To explain Figure 18 in different words, it shows the influence of the calculated joint correction $\Delta\mathbf{X}$ on the uncorrected measured absolute accuracy. Unfortunately, it is difficult to distinguish the uncorrected and corrected points from a gray scale image. The seemingly randomly scattered points throughout the plot represent the error between the desired end-effector position and the measured end-effector position. Then, by applying the calculated $\Delta\mathbf{X}$ to each of the points, the resulting errors are shown to converge within an error sphere of approximately 10 mm.

3.4 Integration of BSC and GEC

To demonstrate the effectiveness of the GEC method, it was implemented in conjunction with the BSC algorithm. Otherwise, GEC applied to a manipulator with poor repeatability would result in absolute accuracy errors that derived from both geometric

errors as well as pure repeatability errors. The results would be impossible to decouple into their respective origins. The control method shown in Figure 19 was created to allow GEC to act on a powerful, yet highly repeatable, manipulator. The goal was to attain absolute position accuracy on the order of the system repeatability.

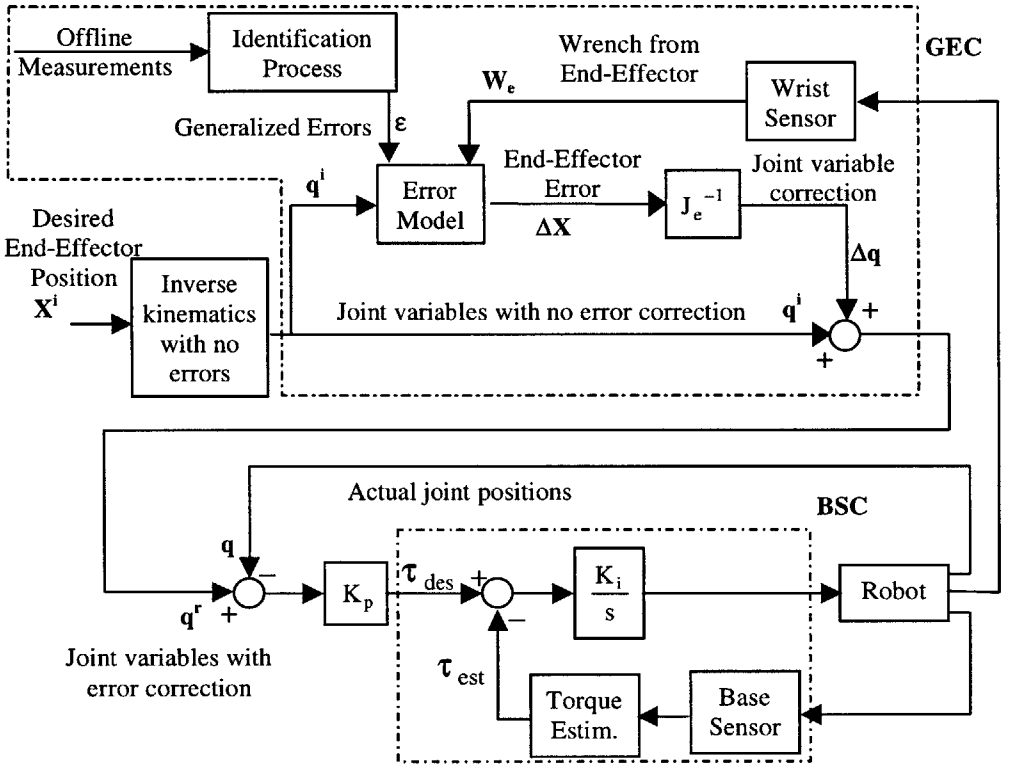

Figure 19 - Base Sensor Control and Error Compensation Scheme

An experiment was conducted to demonstrate the application of the combined BSC and GEC algorithm. The Schilling was commanded to a series of 11 points in the same plane under pure BSC control and then with the addition of two forms of the GEC method. The uncorrected data showed absolute accuracy errors of 29.5 mm (RMS), which are of the same order as the 34.3 mm (RMS) error found from the theodolite measurements. The implementation of GEC with constant generalized errors in their frames resulted in errors being reduced to 11.4 mm (RMS). By expanding the GEC

algorithm to include second order polynomials, absolute positioning errors were further reduced to a RMS value of 8.2 mm.

Figure 20 shows the dramatic improvement in absolute position tracking by using a polynomial GEC algorithm over the uncorrected method. Each of the 11 ideal points is enclosed by a 5 mm radius circle, since the absolute position accuracy is limited by the resolution of the position sensors. Lines connect the measured points to suggest the path of motion and to aid in distinguishing the three implementations. The GEC algorithm also corrected for errors perpendicular to the plane of the points, and these values were measured and included in the error calculations. It can be seen that residual errors are approaching the levels of the resolver electronics. With this improvement in absolute positioning performance, it makes such tasks as the nozzle dam insertion feasible for inherently inaccurate manipulators.

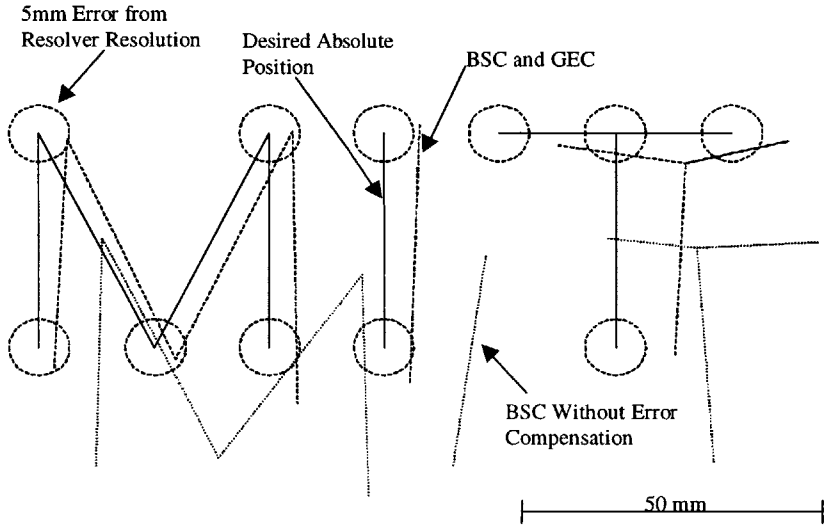

Figure 20 - Uncompensated and Compensated Accuracy

Chapter 4

A Virtual Environment Teleoperator Interface

4.1 Background

A manipulator well suited to the nozzle dam placement task is comprised of a mechanical and electrical system as described in Chapter 2 and uses high precision control algorithms as described in Chapter 3. However, the system is still missing a crucial component, an appropriate operator interface.

Teleoperation is still accepted as one of the most reliable manipulator planning/control methods. It provides the wealth of experience that a human operator brings to a situation, while maintaining a critical check on a system which often lacks the "common sense" to recognize situations when automated control algorithms stray from their intended course of action. Also, human operators can adapt to hard to characterize variations in the task that might prevent automated approaches from succeeding. For these reasons, current attempts to automate the nozzle dam placement task still include a human teleoperator.

Because of the tight workspace and the dangerous environment, it is impractical to place the operator in the steam generator with the Schilling manipulator. However, by removing the operator from the workspace, the ability to visualize the environment is compromised. Therefore, a teleoperation interface must be created. The most common solution is to position a camera in the workspace, thereby providing the teleoperator with a real-time video feed showing the current state of the manipulator and the task. Yet, this allows very limited visualization of the workspace. The large nozzle dam in the confined

environment obscures the views of the mating features. Adding more cameras can improve operator visibility, but an increased number of cameras makes it harder for the teleoperator to process the expanding amount of visual data. Also, each camera increases the cost of the system and requires additional setup time.

A potential teleoperation solution is a virtual, 3-D representation of the environment which is updated in real-time through sensor information acquired from the actual system. This could dramatically improve visual capabilities with arbitrary camera angles, unlimited panning and zooming, as well as the ability to make objects transparent that would otherwise obscure crucial visual features.

4.2 A Kinematic Simulation of the Schilling

Dr. Byung-Hak Cho, a research scientist at KEPRI, spent a year working in the Field and Space Robotics Laboratory. Along with contributing much insight into the current nozzle dam placement methods and the task requirements, he devoted the majority of his time to developing a 3-D kinematic simulation of the nozzle dam placement task as shown in Figure 21. It required a motion file which was processed by the simulation and thereby directed the motions of the virtual Schilling manipulator in a virtual environment where it places and removes a nozzle dam from the steam generator nozzle ring (Cho, 1998). The initial goal of this simulation was to provide a tool for nozzle dam task analysis and to potentially perform trajectory generation.

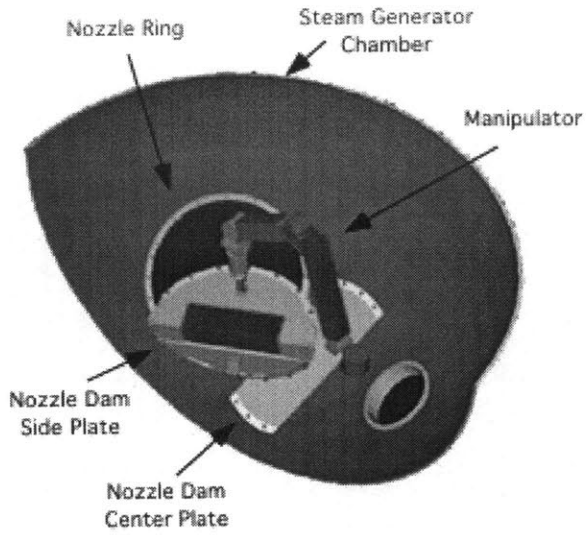

Figure 21 - Simulated Nozzle Dam Placement in Steam Generator

The simulation was programmed in C and compiled with Turbo C++. SVGACC, a shareware graphics library, provided the tools to rapidly develop Super VGA graphics (Balkum, 1996). Using this library, procedures were developed that allow the generation of specific objects including rectangular rods and circular rods. These objects are graphically displayed to the operator using a modified Z-buffer projection rendering algorithm (Cho, 1998). Based on the current camera, the 3-D polygon and its position relative to other polygons, a rendered image is created on the screen which provides a 3-D perspective on a 2-D display. Motion is generated by stop-motion-animation where the 2-D display is alternately writing to two memory pages. When the new page replaces the old page, the next animation frame is displayed to the user. The forward and inverse kinematics of the Schilling manipulator were closely studied to accurately represent the robot in the virtual environment. Fortunately the Schilling is designed so that there is a closed form upper and lower arm solution to the inverse kinematic problem.

As described in Chapter 2, the testbed built in our lab embodied the major design criteria of the actual system, yet was not a complete replica. Therefore, an alternate

virtual environment was designed after the experimental environment as it exists in our lab. Figure 22 shows the manipulator and experimental testbed for both real and simulated systems.

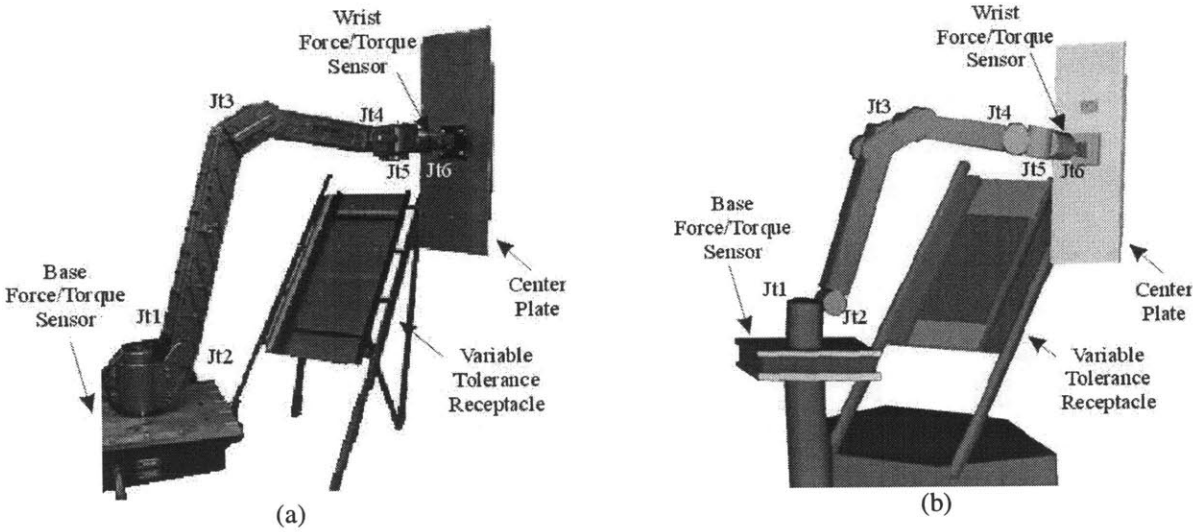

Figure 22 – Real (a) and Simulated (b) Experimental System

The interface provides improved operator visibility by allowing virtual viewing of the workspace using arbitrarily positioned virtual cameras. The virtual cameras also allow for unrestricted panning and magnification of mating edges or other crucial features. Virtual objects can also be made transparent to reveal otherwise physically obscured regions. Figure 23a shows a mating problem that would be difficult to visualize with the human eye or traditional camera system. Although the virtual camera allows the region of interest to be the focus of the display, the configuration of the Schilling manipulator results in the region being obscured. Figure 23b demonstrates the effectiveness of making objects transparent rather than requiring camera angle modification.

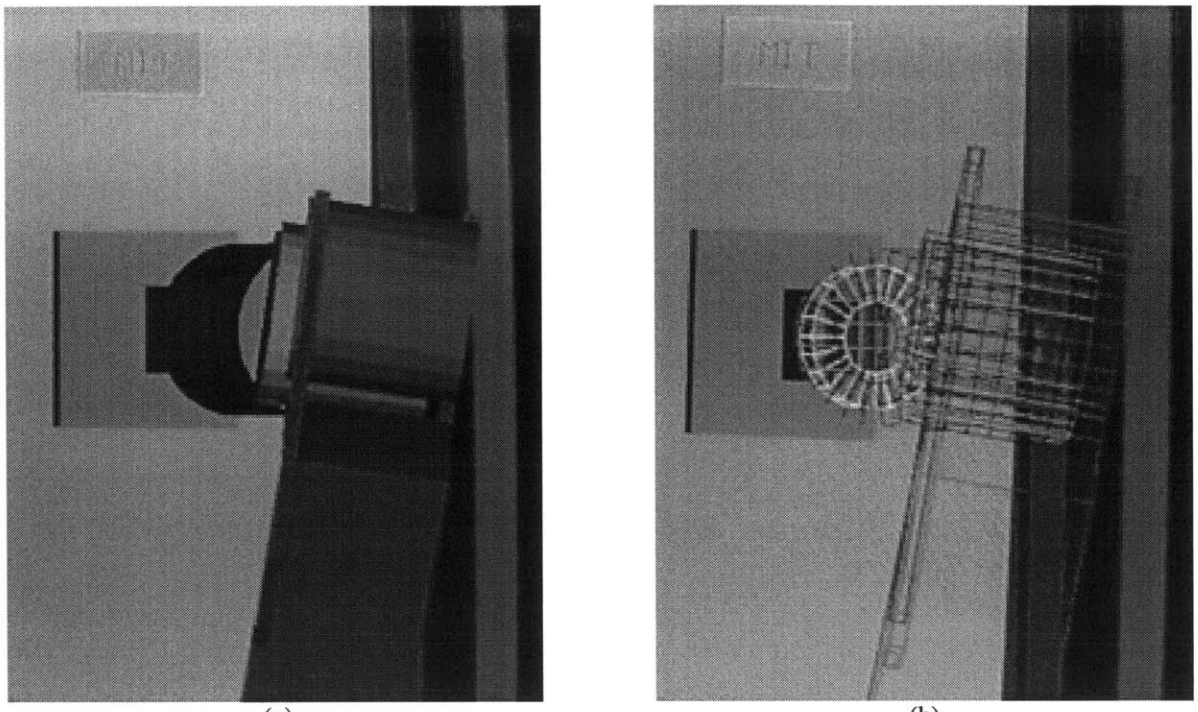

(a) (b)

Figure 23 – Capability of Virtual Cameras and Wire Frame Functionality

4.3 A Virtual Environment Teleoperator Interface

The ideal operator environment is an integration of visualization software with a control system. Once the visualization package was ported to the control PC, the virtual environment could be linked to the actual experimental system. The interface was achieved in three stages.

First, optical theodolites were used to measure the experimental system's position in 3-D space with respect to the base of the Schilling manipulator. The optical theodolites measurements were accurate to within 0.3mm, putting the alignment of the virtual and real environments within the limits of the mating tolerances. Therefore, successful positioning of the virtual nozzle dam within the virtual nozzle ring should correspond to successful insertion in the real system.

The second stage of the integration was to link the virtual Schilling's configuration to that of the real Schilling manipulator. This was achieved by updating the virtual joint angles with the Schilling's actual joint angle readings. An offset vector was created in the simulation software to correlate the virtual and actual home positions of the Schilling. This resulted in a real-time tracking system where the virtual Schilling would mirror motions of the real Schilling manipulator. This system allows the PC to function as a visualization tool for the nozzle dam task, however, the interface was taken one step further.

The final stage allows active control of the Schilling from the teleoperator package. The forward and inverse kinematic relations in the visualization software were used to implement Cartesian end-point control of the robot. Based on a desired end-effector position, the desired joint angles are calculated based on a higher level trajectory planner. The desired joint angles are compared to the current joint positions read from the PMAC's DPRAM. The difference between the desired and actual joint positions is used to generate commands which are written to the PMAC's DAC. The control loop was embedded in an Interrupt Service Routine (ISR) triggered by an interrupt signal originating from a timer card. This guaranteed a consistent sample rate which was set at 10 ms (see Section 2.2.2).

Once the control shell was in place, the control algorithm could be expanded as needed. The tight tolerances of the task require the teleoperator to command fine position adjustments, therefore BSC (Morel, 1996) was implemented to improve the manipulator repeatability through accurate joint torque control using the base force/torque sensor. To improve the correlation of the commanded Cartesian position of

the Schilling and the actual position of the Schilling end-effector, Geometric and Elastic Error Compensation (GEC) was included to improve the absolute accuracy (Meggiolaro, 1998).

However, even with these key enabling technologies, some geometric uncertainty still exists between the modeled and real environments, making teleoperation difficult to perform. It also may not be feasible to resolve the workspace configuration to 0.3 mm as was possible with the optical theodolites. In the case where geometric uncertainty still prevails, alternate methods must be explored to utilize additional information. The method explored in this research displays the contact forces to the operator through the operator interface to aid in the insertion task. These contact forces are calculated from measurements from a wrist force/torque sensor.

Chapter 5

Force Directed Control for Insertion

5.1 Background

The nozzle dam task may still be impossible to complete due to misalignment of the virtual and real environments. Several sources of geometric uncertainty could contribute to this. First, the position of the manipulator relative to the nozzle ring may not be known to within the tolerances of the fit. Second, placing the manipulator in the workspace may require mounting it on a gantry system which is often subject to deformations, thereby inducing errors in the absolute position of the robot end-effector (Mavroidis, 1997). Also, the coupling between the gripper of the manipulator and the nozzle dam may not be repeatable to within the acceptable insertion errors.

For cases where the relative geometry may not be known to within the mating tolerances, a force directed approach can be used to achieve successful completion of the task. There are two major control approaches using force information. One is continuous feedback sensing where the force measurements are directly included in the control loop (Gorinevsky, 1998). The alternate method is a logic branching approach where specific actions are taken based on force measurements matching predetermined cases (Whitney, 1987).

Continuous feedback force controlled insertion in 2-D typically use a mechanical concept called Remote Center Compliance (RCC) where forces can be uniquely mapped into corrective actions that lead to the successful insertion of a peg in a hole (Asada, 1986). The implementation can be demonstrated on continuous servo stiffness control

loops. However, an RCC approach for 3-D is difficult because each plane in the 3-D system can result in RCCs which do not coincide. This would lead to an unstable control law. Also, the wrist force/torque sensor installed in the Schilling has a significant amount of noise that could contribute to instability in continuous feedback. Performing substantial filtering of the wrist sensor could improve the signal quality, but may contribute enough phase delay to drive the system to instability. Alternatively, the logic branching approach was explored.

As mentioned in section 4.1, current attempts at nozzle dam insertion are being done by teleoperation. Therefore, the primary focus of this research is how force information can aid in directing a teleoperator toward successful insertion. However, the last section of this chapter discusses autonomous insertion. Whether the task will be conducted by teleoperation or autonomous algorithm, the magnitude and point(s) of contact must first be calculated.

5.2 Contact Force Estimation

A wrist force/torque sensor provides limited information, namely three force and three torque components, while each contact point is associated with nine unknowns: the coordinates of the contact point location and the contact wrench components. In the case where there is only one contact point with the environment and where the contact torque is zero, it is possible to calculate the contact information required for control. This can be obtained by combining wrist force/torque information with knowledge of the geometry of the mating parts.

Figure 24 shows a plate attached to the end-effector of a manipulator. The force exerted by the environment on the plate, $\mathbf{F_c}$, and the contact location with respect to the wrist force/torque sensor, $\mathbf{r_c}$, can be calculated from:

$$F_c = F_s \tag{5-12}$$

$$r_c = \frac{F_s \times M_s}{\|F_s \times M_s\|} \frac{\|M_s\|}{\|F_s\|} + \alpha F_s \tag{5-13}$$

where $\mathbf{F_s}$ and $\mathbf{M_s}$ are respectively the forces and moments measured from the wrist sensor, and α is an arbitrary constant. Note that Equation (5-13) has an infinite number of solutions, since two equal forces along the same line of action result in the same wrist sensor reading (see Figure 24).

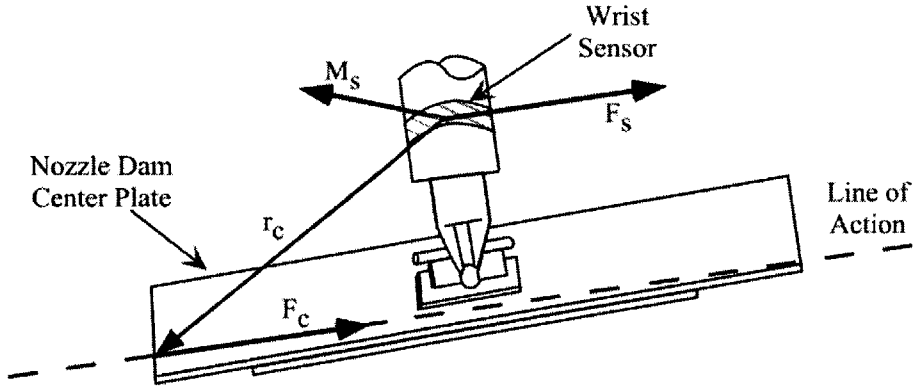

Figure 24 - Contact Force and Wrist Force/Torque Sensor Readings

To obtain a unique solution to Equation (5-13), the plate and receptacle geometry must be considered. Defining Γ as a vector function representing the plate surface in the wrist sensor coordinates, then α is determined by calculating the intersection between the line of action of the contact force and the plate surface Γ.

$$\alpha \mathbf{F_s} \equiv \Gamma - \frac{\mathbf{F_s} \times \mathbf{M_s}}{\|\mathbf{F_s} \times \mathbf{M_s}\|} \frac{\|\mathbf{M_s}\|}{\|\mathbf{F_s}\|} \tag{5-14}$$

Due to the nature of contact forces, which are directed toward the interior of the plate, the calculated values of $\mathbf{r}_c$ must also satisfy

$$\mathbf{n}(\mathbf{r}_c) \cdot \mathbf{F}_c \leq 0 \tag{5-15}$$

where $\mathbf{n}(\mathbf{r}_c)$ is the normal vector to the plate surface at the point $\mathbf{r}_c$.

If Γ represents a convex surface, then the solution to Equations (5-14) and (5-15) is either unique or non-existent. Otherwise, multiple solutions exist for certain configurations. For the particular case shown in Figure 24, Γ is not convex, but it can be represented by a set of simple equations of the planes of the plate. Frequently, as in the case of the nozzle dam insertion plate, a single solution for the contact point can be determined by considering the contact friction as well as the geometry of the mating parts.

5.3 Teleoperator Force-Directed Control

Based on Equations (5-14) and (5-15) and models of the plate and receptacle, a force vector and contact point is calculated from the measured wrist wrench and displayed to the teleoperator. Figure 25 summarizes how a force-updated operator interface is combined with the high accuracy BSC position controller to perform the nozzle dam placement task.

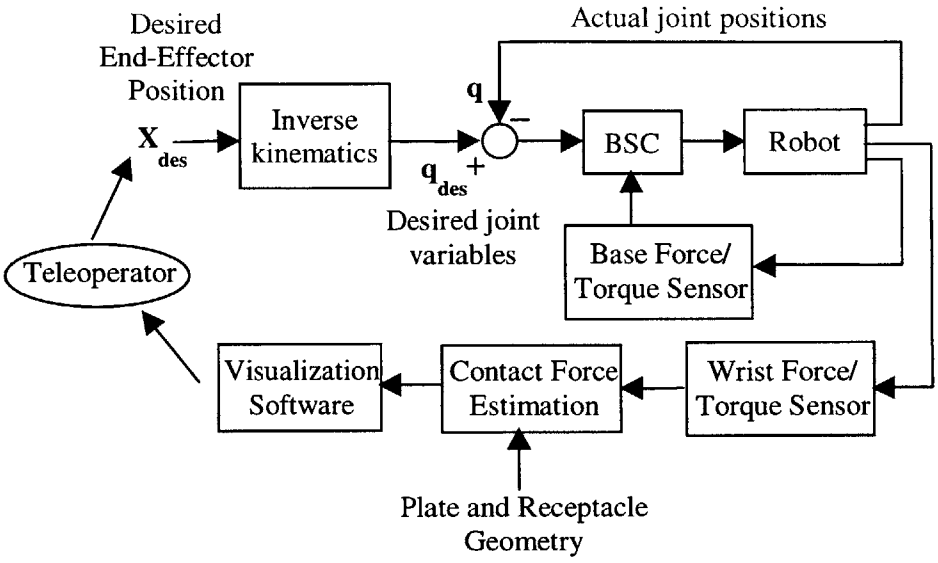

Figure 25 - Base Sensor Control and Contact Force Estimation Scheme

Representative nozzle dam placements were conducted to demonstrate the effectiveness of the force-updated virtual viewing system. Figure 26 shows a sequence of screenshots from the teleoperator display during a typical placement. Each figure shows the center plate contacting the mating receptacle as well as visual feedback of the estimated contact force. The contact vector identifies misalignments in the insertion process, providing the necessary information to command small corrective motions.

Figure 26a suggests translational motions are necessary to align the plate. The next four screenshots shown in Figure 26b-e indicate rotational alignment errors. Finally, the contact force in Figure 26f suggests that successful placement was achieved.

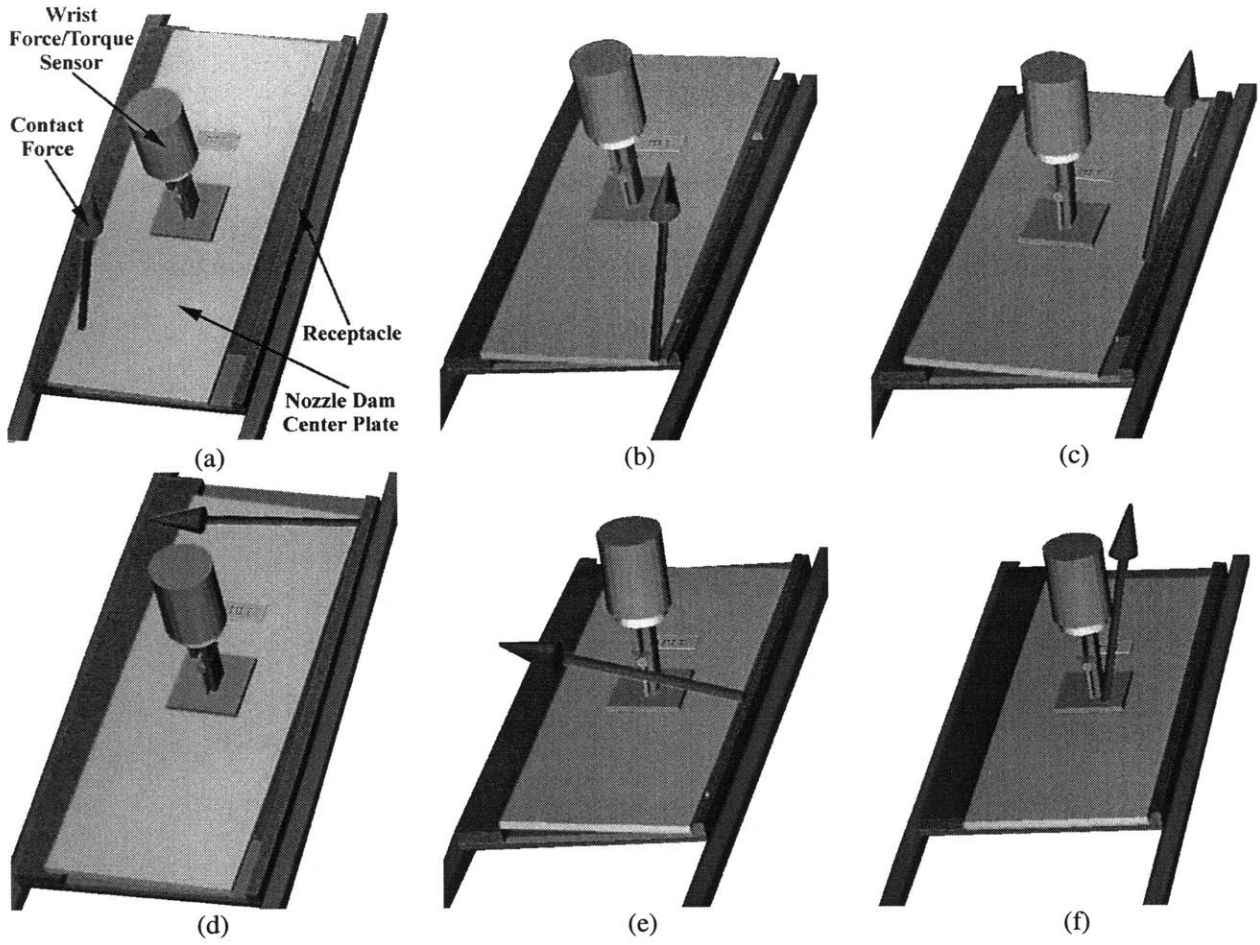

Figure 26 – Typical Placement Steps Using Contact Force Visualization

The experimental insertions show that the force-updated virtual viewing system outlined in Figure 25 allows a conventional hydraulic manipulator to successfully perform the nozzle dam placement task. This approach is made practical since BSC and GEC allow an operator to respond to visual force information with high precision motions.

5.4 Automated Placement

Cursory investigation of automated placement has been conducted, and conclusive results were not found. Teleoperation keeps a human operator in the control loop to prevent possible damage to experimental fixtures, while errors in an automated

control loop combined with the strength of the Schilling manipulator could result in considerable damage. Therefore, to-date, all experiments in automated insertion have been done in simulation.

A software procedure was created for calculating the intersection of rectangular solids. When given two boxes, the procedure would return surface intersections along with the surface normal. Using this procedure, simulations could be conducted for automated placement. The simulated manipulator positions the virtual plate directly above the virtual receptacle and the manipulator is assumed to perfectly track the desired trajectory, however a random displacement and rotation is interjected at the outset. As the placement algorithm attempts to insert the plate, when the solids intersect, the normal to the intersecting surfaces is transformed to the wrist sensor frame, and scaled to represent a force of constant magnitude. The simulated contact force is considered to be the wrist sensor reading, and the automated algorithm specifies new desired coordinates based on that contact force.

To better simulate the actual system, friction and noise components were added. The friction coefficient of aluminum on aluminum was estimated to be 0.2. Therefore a vector, proportional to the normal and in the sense of the current direction of motion, was added to the simulated force measurement. Also added to the force components was random Gaussian noise as characterized and shown in Figure 12.

Two logic branching algorithms were attempted. The first, and least successful of the two, attempted to directly insert the plate, and when presented with a contact force and contact point, generated a new desired position based on a set of rules. The second, and more successful, used an exploratory approach where the insertion plate was

intentionally pitched by a known amount. It was then moved in what was thought to be the normal to the receptacle surface until it ideally would contact the intended corner. That corner was then slid across the receptacle surface until finding a boundary rail. A series of steps were then taken to attempt to align the insertion plate and rotate it into place. Each phase of the placement has memory to attempt to recover when an expected contact is not found after a certain maximum allowed displacement. A force originating from the center off the plate and normal to the surface signified successful placement. However, even this state had to be verified by controlled motions, because incorrect configurations could result in a deceptive force reading. These algorithms are crude, but proved insightful into methods by which a teleoperator might proceed in the insertion process.

Chapter 6

Conclusions and Suggestions for Future Work

6.1 Conclusions

This thesis described the design approach to creating a force-directed control system for the completion of the nozzle dam insertion task. The process involved the application of existing technologies, the necessary modifications to those technologies, and the development of tools that allow all these components to work together in allowing successful insertion of a representative insertion plate within a tight tolerance receptacle.

An experimental system was developed that employed a Schilling hydraulic manipulator, a mechanical fixture that embodied the crucial aspects of the nozzle dam task, and sufficient electronics to support investigation of the problem. A legacy control system was maintained, while additional computation power and sensors were added. The new system allowed the exploration of both high performance control algorithms and advanced operator interfaces.

Control algorithms were implemented to improve system performance. A simplified, model-free form of Base Sensor Control (BSC) was applied to the Schilling manipulator. BSC used a base force/torque sensor to accurately control joint torques, thereby compensating for joint friction. This substantially improved the manipulator's poor position repeatability. The BSC controller was then combined with GEC to compensate for geometric and elastic errors that degraded the absolute positioning accuracy of large manipulators with inherently good repeatability. The results showed

that by applying the combined control algorithm, the absolute accuracy of the Schilling was improved by a factor of 10 over traditional PI controllers. This improved performance allowed the Schilling system to be used for the nozzle dam task.

A robotic visualization and control system was then presented. A visualization software package had been developed with a 3-D kinematic model of the Schilling manipulator and the experimental workspace. This system was interfaced with the data capabilities of the control electronics to create a teleoperator interface. This allowed a user to accurately visualize the task as well as perform active control over the desired position and trajectory of the Schilling end-effector.

Finally, methods were presented that use contact force information between the center plate and its receptacle to aid in the insertion task. Force data is obtained from wrist sensor wrench measurements, contact points can be calculated using knowledge of the mating geometries. The contact force vector is displayed to the teleoperator and allows for real-time recognition and correction of misalignments in the insertion process. This aids in successfully achieving insertion using a teleoperator position control algorithm. Also, automated placement algorithms in simulation were discussed.

This work demonstrates how a strong hydraulic manipulator could achieve the nozzle dam placement task by combining a high accuracy position controller, such as BSC and GEC, with a force-directed teleoperation interface.

6.2 Future Work

Although this thesis presents a specific development of a system designed for the nozzle insertion task, there are areas that have yet to be explored. These include

increased positioning capabilities, improved operator interfaces, and more powerful force control methods.

Although the specific hardware used in this research can place a heavy plate within a receptacle with one millimeter tolerances, there are many applications of powerful manipulators that require even finer position control. An area of interest would be to upgrade the resolver to digital converter boards to a 16-bit converter to acquire the full 0.7 arc min resolution provided by the joint resolvers. The application of BSC and GEC to this system may present new difficulties when trying to drive the manipulator's repeatability and accuracy to the tens of μm threshold.

For the teleoperator interface, there would be considerable interest in extending the system to an even more powerful graphical interface environment. The use of current graphic technologies such as Direct3D would allow increased rendering capabilities while moving the control system into a realm where networking capabilities become available.

The area most open to further research is that of manipulation of the force data. Interesting developments might be to replace the theodolite offline measurements with online calibration using force information and known geometries. Calibration data could be acquired by having the Schilling touch surfaces of a calibration cube or by touching points on the nozzle ring. If the force information can be mapped to a point in 3-D space and the joint angles can be resolved with high accuracy, then data can be acquired and processed automatically to implement the GEC method.

A virtual environment that is updated in real-time would be another area of interest. As the insertion progresses and contact force data identifies misalignments, the virtual environment could be modified to reflect an updated model.

Finally, there are many other possible applications of this technology. The findings and results discussed in this paper could be extended to improve control of underwater robots, space manipulators, and others where high accuracy may be necessary while the environment prevents human operators from entering the workspace.

References

Advanced Mechanical Technology, Inc. (AMTI), "Instruction Manual Model OR6-5 Biomechanics Platform," Newton, Massachusetts, 1991

Asada, H. and Hirai, S., "Towards a symbolic-level force feedback: recognition of assembly process states." *Robotics Research Fifth International Symposium*, pp.341-6, MIT Press, Cambridge, MA, 1990

Asada, H. and Slotine, J.-J., *Robot Analysis and Control*, Wiley, New York, New York, 1986

Balkum, S. and Still, D., "SVGACC Graphics Library Manual," Zephyr Software, 1996.

Bicchi, A., Salisbury, J., and Brock, D., "Contact Sensing from Force Measurements," *The International Journal of Robotics Research*, Vol. 12, No. 3, pp. 249-262, 1993

Canudas-de-Wit, C., Olsson, H, Astrom, K.J., and Lischinsky, P., "A New Model for Control of Systems with Friction," *IEEE Transactions on Automatic Control* Vol. 40, No. 3, pp. 419-425, March 1995

Cho, B.H., "Maintenance Procedure: Nozzle Dam Installation and Removal," KEPCO Internal Report, 1997

Cho, B.H., "Simulation Studies on Robot System Applied to Nozzle Dam Installation," Technical Report to KEPRI, 1998

Craig, J., *Introduction to Robotics*, Addion-Wesley Publishing Company, Massachusetts, USA 1989

Delta Tau Data Systems, Inc., "PMAC User's Manual," Northridge, CA, 1992

Drouet, P., Dubowsky, S., and Mavroidis, C., "Compensation of Geometric and Elastic Deformation Errors in Large Manipulators Based on Experimental Measurements: Application to a High Accuracy Medical Manipulator," *Proceedings of the Sixth International Symposium on Advances in Robot Kinematics*, Strobl, Austria, June 1998

Farahat, A.O., Graves, B.S., and Trinkle J.C., "Identifying Contact Formations in the Presence of Uncertainty," *Proceedings of 1995 IEEE/RSJ International Conference on Intelligent Robots and Systems*, Vol.3, pp.59-64, 1995

Gorinevsky, D., Formalsky, A., and Schneider, A., *Force Control of Robotics Systems*, CRC Press, New York, New York, 1997

Gullapalli, V., Grupen, R., and Barto, A., "Learning Reactive Admittance Control," *Proceedings of the IEEE International Conference on Robotics and Automation*, pp. 1475-1480, 1992

Habibi, S.R., Richards, R.J., and Goldenberg, A.A., "Hydraulic Actuator Analysis for Industrial Robot Multivariable Control," *Proceedings of the American Control Conference*, Vol. 1, pp. 1003-1007, 1994

Hollerbach, J., "A Survey of Kinematic Calibration," *Robotics Review*, MIT Press, Cambridge, MA, 1988

Iagnemma, K., Morel, G., and Dubowsky, S., "A Model-Free Fine Position Control System Using the Base-Sensor: With Application to a Hydraulic Manipulator," *Symposium on Robot Control* (SYROCO '97), Vol. 2, pp. 359-365, 1997

Lee, J.-H., Kim, S., Kim, D., Kang, H., and Park, J.-O., "Teleoperation system for sensitive task manipulation," *Proceedings of the 3rd Asian Conference on Robotics and its Applications*, pp.257-64, 1997

Kuklinski, A., *The Practical Implementation of an Experiment Tool for the Dynamic Interactions in Mobile Manipulator Systems*, S.M. Thesis, Department of Mechanical Engineering, Massachusetts Institute of Technology, Cambridge, Massachusetts 1993

Mavroidis, C., Dubowsky, S., Drouet, P., Hintersteiner, J., and Flanz, J., "A Systematic Error Analysis of Robotic Manipulators: Application to a High Performance Medical Robot," *Proceedings of the 1997 IEEE International Conference of Robotics and Automation*, Vol.2, pp.980-5, 1997

Meggiolaro, M., Jaffe, P., and Dubowsky, S., "Achieving Fine Absolute Positioning Accuracy in Large Powerful Manipulators," *submitted to the IEEE International Conference on Robotics and Automation* (ICRA'99), Detroit, 1999a

Meggiolaro, M., Jaffe, P., Iagnemma, K., and Dubowsky, S., "A Force-Updated Kinematic Virtual Viewing System with Application to Nuclear Power Plant Maintenance," *The Tenth World Congress of the International Federation for Theory of Machines and Mechanisms* (IFToMM'99), Oulu, Finland, 1999b

Meggiolaro, M., Mavroidis, C., and Dubowsky, S., "Identification and Compensation of Geometric and Elastic Errors in Large Manipulators: Application to a High Accuracy Medical Robot," *Proceedings of the 1998 ASME Design Engineering Technical Conference*, September 1998

Merritt, H., *Hydraulic Control Systems,* John Wiley and Sons, New York, New York, 1967

Ming, O.-Y., Beard, D.V., and Brooks, F.P. Jr., "Force display performs better than visual display in a simple 6-D docking task," *Proceedings of the 1989 IEEE International Conference on Robotics and Automation,* Vol. 3, pp.1462-6, 1989

Minsky, M., Ming, O.-Y., Steele, O., Brooks F.P. Jr, and Behensky M., "Feeling and seeing: issues in force display," *Computer Graphics, V*ol.24, No.2, pp.235-43, March 1990

Morel, G. and Dubowsky, S., "The Precise Control of Manipulators with Joint Friction: A Base Force/Torque Sensor Method," *Proceedings of the IEEE International Conference on Robotics and Automation*, Vol. 1, pp. 360-365, 1996

Nevins, J.L. and Whitney, D.E., "The Force Vector Assembler Concept," *1st CISM-IFTOMM Symposium on Theory and Practice of Robots and Manipulators*, pp.21, 1973

NuDAQ, "ACL-8454 Multi-Functions Counter/Timer Card," 1996

Qiao, H., Dalay, B.S., and Parkin, R.M., "Fine Motion Strategies for Robotic Peg-Hole Insertion," *Proceedings of the Institution of Mechanical Engineers*, Part C, Vol. 209, pp. 429-448, 1995

Popovic, M.R., Shimoga, K.B., Goldenberg, A.A., and Hui, R.C., 1994, "Model-Based Compensation of Friction in Direct Drive Robotic Arms." *Journal of Studies in Information and Control*, Vol.3, No.1, pp.75-88, March 1994

Pfeffer, L.E., Khatib, O., and Hake, J., "Joint Torque Sensory Feedback of a PUMA Manipulator," *IEEE Transactions on Robotics and Automation*, Vol. 5, No. 4, pp. 418-425, 1989

Roth, Z.S., Mooring, B.W., and Ravani, B., "An Overview of Robot Calibration," *IEEE Southcon Conference*, Vol.RA-3, No.5, pp.377-85, Oct. 1987

Schilling Development, Inc., "Tomcat Manipulator System," *Technical Manual*, Davis, CA, 1991

Schneiter, J.L., *Automated Tactile Sensing for Object Recognition and Localization*, PhD Thesis, Department of Mechanical Engineering, Massachusetts Institute of Technology, Cambridge, Massachusetts, 1986

Simunovic, S.N., *An Information Approach to Parts Mating*, PhD thesis, Department of Mechanical Engineering, Massachusetts Institute of Technology, Cambridge, Massachusetts, 1979

Vaillancourt, C. and Gosselin, G., "Compensating for the Structural Flexibility of the SSRMS with the SPDM," *Proceedings of the International Advanced Robotics Program*, Second Workshop on Robotics in Space, 1994

VMEbus User's Handbook, CRC Press, Boca Raton, FL, 1988

Volpe, R. and Khosla, P., "An Analysis of Manipulator Force Control Strategies Applied to an Experimentally Derived Model," *Proceedings of the 1992 IEEE/RSJ International Conference on Intelligent Robots and Systems*, pp.1989-1997, 1992

Wind River Systems, "VxWorks Programmer's Guide," Emeryville, CA, 1991

Whitney, D.E., "Historical Perspective and State of the Art in Robot Force Control," *The International Journal of Robotics Research*, Vol. 6, No. 1, pp.3-14, Spring 1987

Zezza, L.J., "Steam Generator Nozzle Dam System," *Transactions of the American Nuclear Society*, Vol. 50, pp. 412-413, 1985

Appendix A

Driver Code Prototypes

This appendix contains function prototypes and descriptions of the driver code for the PC VME link. This would be useful for writing new code on the PC that interfaces with the VMEbus.

A.1 PC VME Link

int pcvme_link_initialize()
{
Resets the VME link. Returns 1 if error, 0 otherwise. Must be run once at beginning of program.
}

*int VMEIn(unsigned long vme_addr, int *vme_data, char a24)*
{
Stores 16-bit data from vme_addr in the 16-bit address space (a24 false) or 24-bit address space (a24 true) into pointer vme_data. Returns non-zero if error occurs.
}

int VMEOut(unsigned long vme_addr, int vme_data, char a24)
{
Writes vme_data into vme_addr in the 16-bit address space (a24 false) or 24-bit address space (a24 true). Returns non-zero if error occurs.
}

Appendix B

Wrist Force/Torque Sensor Wiring Description

The following are pin-outs for the interface between the wrist force/torque sensor and the Data Translation ADC.

B.1 Connector Diagram

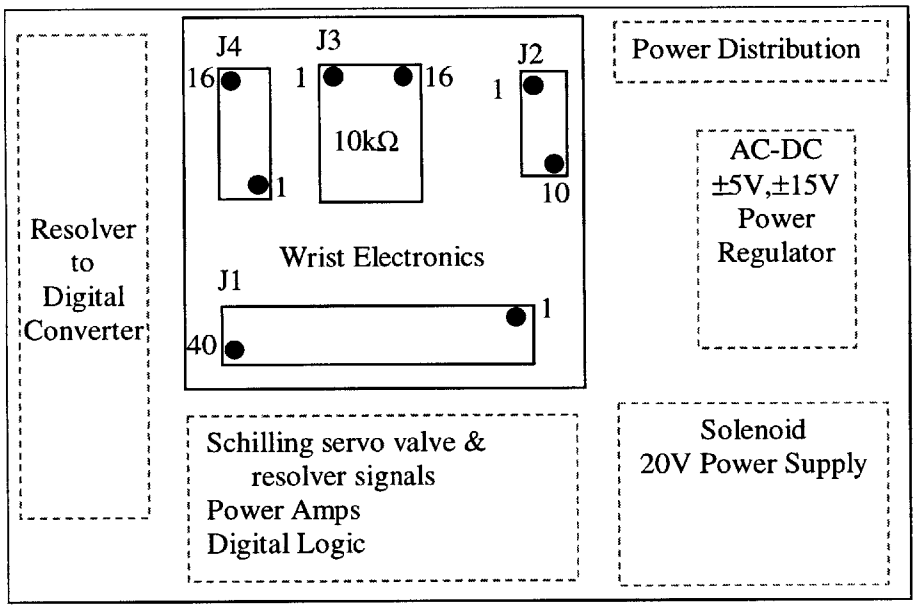

Figure 27 - Schilling Interface Electronics

B.2 J1 Connector from Schilling

J1 (from Schilling)	Connect to	Description
1	NC	Jaw1 Pressure +
2	NC	Jaw1 Pressure -
3		Shield
4	J4-7	VBV+
5	J4-8	VBV-
6		Shield
7	J4-1	VAH+
8	J4-2	VAH-
9		Shield
10	J4-9	VCH+
11	J4-10	VCH-
12		Shield
13	J4-13	VDH+

14	J4-14	VDH-
15		Shield
16		Jaw2 Pressure +
17		Jaw2 Pressure -
18		Shield
19	J2-2	+5
20	J2-3	-5
21		Shield
22	J4-11	VCV+
23	J4-12	VCV-
24		Shield
25	J4-3	VAV+
26	J4-4	VAV-
27		Shield
28	J2-4	+15
29	J2-5	-15
30		Shield
31	J4-5	VBH+
32	J4-6	VBH-
33		Shield
34	J4-15	VDV+
35	J4-16	VDV-
36		Shield
37	J2-1, J4-17	GND

B.3 J2 Power Connector

J2 (Power)	Description
1	GND
2	+5
3	-5
4	+15
5	-15
6	NC
7	NC
8	NC
9	NC
10	NC

B.4 J3 10 kΩ Resistor Bank

J3 (Resistor Bank)	Connect to	Description
1	J1-8	VAH-
2	J1-26	VAV-
3	J1-32	VBH-
4	J1-5	VBV-
5	J1-11	VCH-
6	J1-23	VCV-
7	J1-14	VDH-
8	J1-35	VDV-
9	J3-10	GND
10	J3-11	GND
11	J3-12	GND
12	J3-13	GND
13	J3-14	GND
14	J3-15	GND
15	J3-16	GND
16	J2-1	GND

B.5 J4 Signal Connector to ADC

J3 (Resistor Bank)	Description
1	VAH+
2	VAH-
3	VAV+
4	VAV-
5	VBH+
6	VBH-
7	VBV+
8	VBV-
9	VCH+
10	VCH-
11	VCV+
12	VCV-
13	VDH+
14	VDH-
15	VDV+
16	VDV-